

Article

# Sensitivities in Wind Driven Spectral Wave Modelling for the Belgian Coast

Frans van Eeden <sup>1,\*</sup>, Georgios Klonaris <sup>1</sup>, Jeffrey Verbeurgt <sup>1</sup>, Peter Troch <sup>2</sup> and Alain De Wulf <sup>1</sup>

<sup>1</sup> Department of Geography, Ghent University, BE-9000 Ghent, Belgium

<sup>2</sup> Department of Civil Engineering, Ghent University, BE-9052 Zwijnaarde, Belgium

\* Correspondence: frans.vaneeden@ugent.be

**Abstract:** This paper presents the analysis of spectral wind-wave modelling (using SWAN) of the North Sea focusing on the modelled wave parameters along the Belgian coast. Two wind databases were used to drive the model: ECMWF-ERA5 reanalysis and the Dutch Offshore Wind Atlas. The models were calibrated with measured data at various stations along the Belgian coastline. The accuracy in terms of wave parameter statistics was compared for the calibrated and uncalibrated models. It was found that a calibrated SWAN model does, in general, produce more accurate results when compared to measured data for stations along the Belgian coastline even though not by any significant margin. Comparing the two wind databases, on the modelling scale conducted in this study, there is no advantage observed in using a spatially finer scale wind database over a coarser database to force the model. The grid sizes were varied in the models and marginal differences were observed in the modelled data. The long-term extreme value statistics were calculated for various grid sizes and compared to published values. It is shown that the extreme value statistics are relatively insensitive to the grid density and thus much time can be saved on long-term modelling on this model scale. In addition, a benefit to the practise of grid nesting is demonstrated when considering complex bathymetric effects that have an influence on wave transformation in the shallower areas of the coast, especially along the Belgian coastline demarcated with its numerous sandbanks.

**Keywords:** SWAN; Belgium; wave modelling; wind-waves; ECMWF-ERA5; DOWA



**Citation:** van Eeden, F.; Klonaris, G.; Verbeurgt, J.; Troch, P.; De Wulf, A. Sensitivities in Wind Driven Spectral Wave Modelling for the Belgian Coast. *J. Mar. Sci. Eng.* **2022**, *10*, 1138. <https://doi.org/10.3390/jmse10081138>

Academic Editor: Theophanis V. Karambas

Received: 19 July 2022

Accepted: 16 August 2022

Published: 18 August 2022

**Publisher's Note:** MDPI stays neutral with regard to jurisdictional claims in published maps and institutional affiliations.



**Copyright:** © 2022 by the authors. Licensee MDPI, Basel, Switzerland. This article is an open access article distributed under the terms and conditions of the Creative Commons Attribution (CC BY) license (<https://creativecommons.org/licenses/by/4.0/>).

## 1. Introduction

Economical coastal engineering design, which is intent on reducing failure risk and the frequency of maintenance, is highly dependent on the quality of the input to the design parameters. Structural coastal engineering requires future projected extreme events [1] while beach stabilisation demands long-term operational conditions for its design to be manageable and sustainable [2].

The quality of the inputs to the design formulas has a direct influence on the inherent risk of design failure and, as a result, the economy of the design. In order to minimise the design risk and improve the service life of the structure, design and maintenance input with an acceptable amount of certainty is needed. The uncertainty inherent in coastal engineering design is complicated by the dynamic coastal processes and resulting forces that are often difficult to project into the future. After all, the only available reliable data is from the past. In engineering practise, numerical models are utilised in order to quantify design data for future long-term statistical probable events.

Over a vast region, as encompassed by the North Sea, limited options for numerical forcing from actual wind and/or wave measurements are available. Apart from the spatial sparsity of the available measurements, the temporal variation in the duration and measurement periods, and the fact that the data is managed by a number of different governments and/or private entities (e.g., platform operators, wind farm operators, etc.), makes this option non-feasible from a modelling perspective.

In order to bridge this problem, global scale atmospheric numerical models are used to produce hindcast datasets of various meteorological and marine parameters using historical data and validated against measurements. Not only are these datasets temporally and spatially consistent, they are also deemed reliable in an assimilated manner where global observations are combined with model data [3]. In typical engineering design, hindcast data sets are used for model calibration and to produce long-term hindcast modelled wave parameter databases while using observed/measured data as validation for the modelling exercise. In most cases, the data required to force the models are available, however, the inherent uncertainty with regard to their accuracy is not always known.

In essence, the quality of wind-wave modelled results is dependent on the quality input forcing parameters, which, in this case, is the wind [4]. This is even more pertinent when a semi-enclosed basin, as the case with the North Sea, is considered where the main wave generation mechanism is wind-generated waves, especially during storm conditions and related storm surges. Not only are the wave heights an important factor but also the wave directions due to the geometry of the North Sea where a change in wind direction alters the wind fetch and, as a result, alters the wave characteristics ([5,6]).

It is acknowledged that near-surface wind fields (say  $U_{10}$  is the wind velocity at 10 m height above the mean sea level) are by-products of meteorological models and not necessarily the main focus of global atmospheric model output [7] which leads to, inter alia, a significant variation in spatial wind density, generated by the various meteorological products available (e.g., NOAA, ECMWF, KNMI). This stems mainly from the challenge of collecting measurements over a vast ocean and validating the near-surface parameters by re-tuning the model specifically for this purpose [8]. In addition, due to the limited scale of the numerical atmospheric models, there inherently exists a good representation of the synoptic variability scales but not of the smaller scales. Further, the wind at an arbitrary height ( $U_{10}$ ) is characterised in terms of averages even though much variability exists over the averaged time frame. Most atmospheric products report these averages in hourly or 3-hourly increments [9]. Other factors that define the structure of the wind are the geography of the area under consideration where the land/sea interface, orographic effects, sheltering effects and sea-breeze may cause a complicated wind structure that directly influences the local wave conditions. These conditions are even more exacerbated by semi-enclosed basins where spatial boundaries are defined by land masses [10].

In order to take into account the mesoscale and small-scale variability in the wind, the temporal and spatial resolution of the atmospheric models must be refined. However, this comes at a high computational cost in addition to sensitivities to errors in the initial and boundary conditions [10]. Higher resolution wind model output can be achieved by Limited Area Models (LAM) such as LAMI or COAMPS, which have proved to produce more accurate wave modelling results within the context of an enclosed narrow sea (Adriatic Sea) when compared to a coarser gridded atmospheric model wind output (i.e., ECMWF T511). The fact that the higher resolution models contain a more accurate representation of the orography is cited as the main reason for the increased accuracy [7]. In general, Mass et al. (2002) [11] reports that the representation skill of storms, sharper mesoscale features and convective events increases with an improvement of atmospheric model resolution.

However, an arbitrary increase in LAM model grid resolution (nested in a global atmospheric model) does not necessarily result in a more accurate model. Instead, the relationship between the parent (global model) and child model (LAM) is important for the resulting accuracy of the wave model as inherent errors in the parent model can propagate into and be processed in the LAM. This was further confirmed by using the fully coupled WAM [4] wave model to calculate the wave heights given the various wind input resolutions [12]. The authors found that an increase in modelled wind field resolution used as input to the wave model, in general, improves the modelled wave parameter accuracy. However, Cavaleri [13] pointed out that, even with an increase in the “quality” of the wind used for input into the numerical models, the wind-wave models fail to simulate

the peak wave heights of significant storm events. The reasons stated by Cavaleri are not trivial matters as he presents a fine balance between model components representing the wind-wave generation physics, the numerical discretisation (and associated assumptions) and the wind input [13] (see also the paper presented by the WISE group [14]). Within the context of storm wind conditions, Bricheno et al. (2013) [15] showed that by increasing the atmospheric forcing model resolution from 12 km to 4 km, an increase in the modelled peak wave heights was observed (using the wind-wave model WAM) in addition to an increase in wave direction skill for the Irish Sea. The authors did not extend their wind-wave model domain to include fetch-limited scenarios where the modelled wave conditions are attuned by local winds.

Lavidas et al. (2017) [16] report on calculations from the SWAN numerical wave models (TU-Delft, ref. [17]) covering the North of Scotland forced by ECMWF ERA-Interim Re-Analysis wind (6-hourly data at  $0.125^\circ$ ) and the National Centre for Atmospheric Research and the National Oceanic and Atmospheric Administration (NOAA) CFSR-NCEP Re-Analysis dataset (hourly at  $0.30^\circ$  grid spacing) for the year of 2010 were compared to each other. An increase in the spatial resolution of the wind having an impact on the accuracy of the model was confirmed; however, no quantification of the relative influence of the temporal resolution on the modelling accuracy was made. Using the SWAN wave model, a numerical wave model across the Red Sea was forced with variable spatial and temporal resolutions sub-sampled from the same source, i.e., the GFS4\_anl wind product from the NOAA, it was concluded that the spatial resolution has a more significant influence on the resultant wave modelling accuracy compared to the temporal resolution [18]. In addition to the spatial resolution of the input wind forcing playing a significant role, the temporal resolution is another obvious factor that has been investigated [16].

In the literature presented, all indications are present that an increase in spatial and temporal resolution of the wind input to a numerical wind-wave (phase averaging) model will lead to an increase in the accuracy of the modelled wave parameters.

However, the question remains as to what degree of detail the wind input has to be quantified in order to calculate reliable long-term wave parameters under strictly wind forcing. In addition, spectral wind-wave models underestimate the wave peaks during significant wave events, according to Cavaleri and the WISE group ([10,13,14]). Bear in mind that the North Sea area is a semi-enclosed basin where fetch-limited winds and local winds have an influence on the local wave climate on a much smaller scale than coastlines along open oceans. Regardless of all the limitations and approximations inherent to numerical models, Cavaleri does cite the most obvious improvement that can be made, which is an increased resolution of the wind input to the numerical models.

Apart from introducing a new set of physics into the wave model that accounts for the deficiencies inherent in meteorology, the most practical solution for the coastal Engineer is to find and apply the highest quality forcing data he can find. In the context of the North Sea and with a focus on the Belgian Continental Shelf, the question is which available database delivers the most accurate and reliable wave calculations in terms of accuracy given the industry standard numerical models engineers usually work with. Note that within this context, accuracy is defined in accordance with the statistical methods employed.

This study focuses on the accuracy of a spectral wave model (SWAN) relative to measured parameters at specific locations along the Belgian coastline when forced purely by wind over a sufficiently large domain. The benefit, in terms of accuracy and calibration effort, of a calibrated SWAN model relative to an uncalibrated model when forced with the ECMWF-ERA5 Reanalysis ("ECMWF-ERA5") and Dutch Offshore Wind Atlas ("DOWA") are unknown for the Belgian coastline at this scale, specifically whether the "quality" of the wind input data makes a difference in the model results. The interpolation of ECMWF-ERA5 and DOWA wind data onto the SWAN coarse and finer computational grids could result in the loss of small-scale wind information which could influence the accuracy of the model results. The discretisation of the model grid has a great impact on the economy of the computational time of the model. As such, various grid discretisations are implemented

in the SWAN models and compared statistically to gauge the relative accuracy of the model results. Given the computational economy of a coarser grid, the accuracy of long-term extreme value calculations is investigated for a fine and coarse grid forced with both the ECMWF-ERA5 and DOWA wind databases. Finally, grid nesting is implemented in the models and the accuracy for each of the stations is compared with the measured values in order to gauge whether the added complexity and refinement lead to greater statistical accuracy in the results.

This study compares the results of various features (i.e., wind database, calibration status and grid discretisation) configured within a particular SWAN model with measured parameters along the Belgian coast. Table 1 lists the model features varied within each section of this study.

**Table 1.** Various model features investigated.

	Wind Database		Model Calibration		Average Grid Cell Dimension			
	ECMWF-ERA5	DOWA	Calibrated	Uncalibrated	7.5 km	5 km	2.5 km	Nested Grids
Section 4.1: Statistical Comparison	Y	Y	Y	Y		Y	Y	
Section 4.2: LTEVA	Y	Y	Y	Y	Y		Y	
Section 4.3: Grid nesting	Y	Y	Y	Y				Y

## 2. Area of Study

The North Sea is located between the British Isles and the continent of Europe. In particular, it is bordered by England and Scotland to the west, Norway and Denmark in the east and France, Belgium, The Netherlands and Germany in the south. The North Sea is connected to the Atlantic ocean through the English Channel (in the southwest) and the North West Atlantic in the north. With an area spanning approximately 570,000 square km, the North Sea is an important area for shipping and fishing feeding some of the world’s busiest ports, i.e., Rotterdam, Antwerp and Zeebrugge. The bathymetry of the North Sea and adjacent seas is shown in Figure 1 where the shallower regions are indicated by the red colouring. The North Sea is a shallow sea ranging in depths from 200 m in the North to 20 m along the Belgian/Dutch/German coast with an average depth of around 80 m [19].

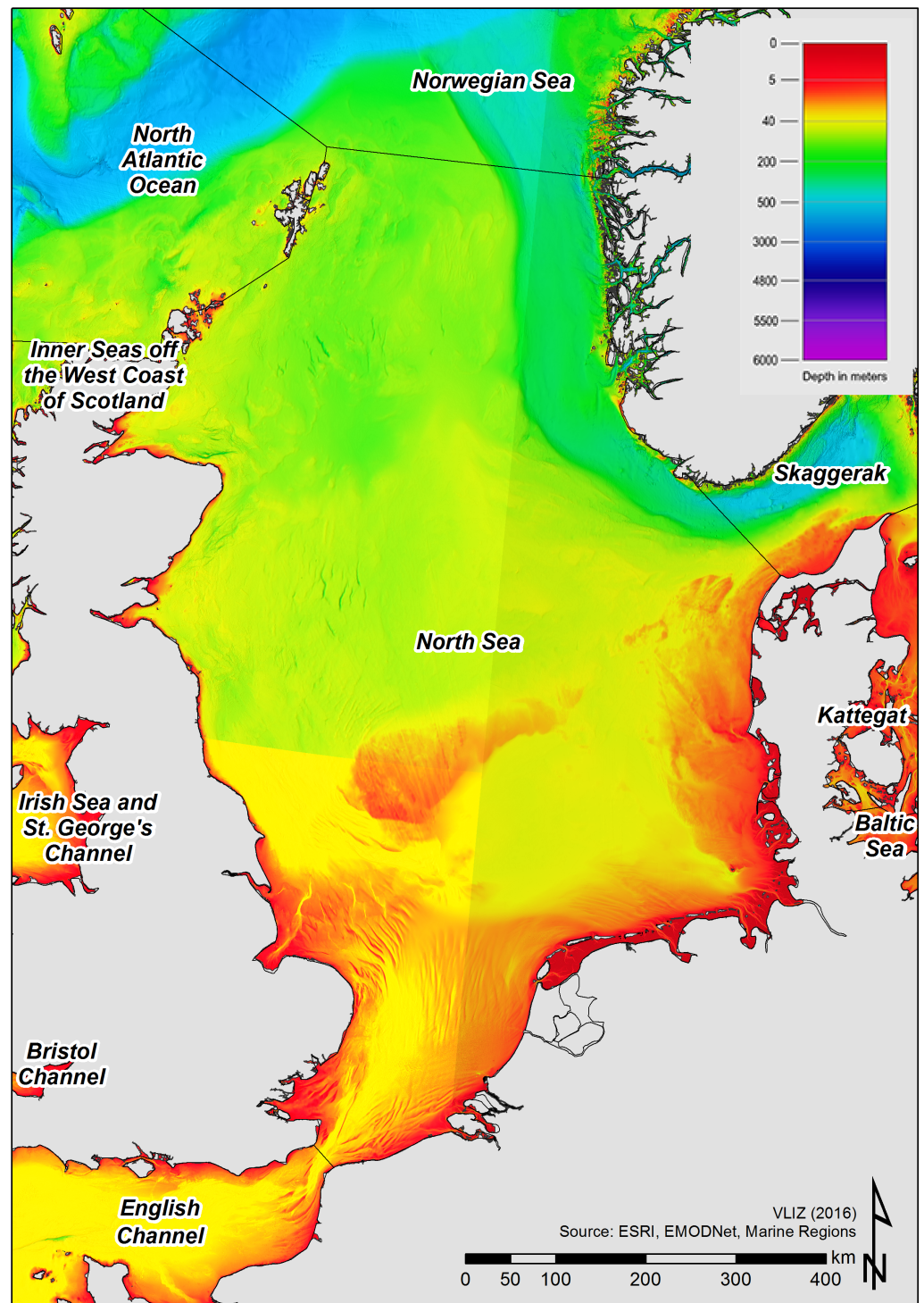


Figure 1. Bathymetry of the North Sea and adjacent seas [20].

### 3. Materials And Methods

#### 3.1. Methodology

When sufficient measured or validated data is available, numerical models are generally calibrated to the data (e.g., buoys, satellite data, etc.), which increases confidence and the level of accuracy of the numerical model results. However, data sufficient to calibrate the model is not always available. This paper looks at various factors that could influence a model's accuracy when compared to physical measured data with a specific focus on the relative accuracy of the wind databases used to force the model.

The first part of this study investigates the accuracy of a calibrated and an uncalibrated numerical wave model, using two wind databases, ECMWF-ERA5 and DOWA. A systematic calibration of the SWAN numerical wave model for the two wind databases was performed by incrementally tuning the coefficients related to the rate of white capping dissipation ( $C_{ds1}$  for the KOMEN formulation and  $C_{ds2}$  for the Janssen formulation). The modelling results are statistically compared to measured values for the period 1 October 2015 to 31 March 2017. Note that the uncalibrated SWAN models assume the default values determined by Komen et al. (1984) [21] and Jansen (1992) [22] (as per Table 2).

These models are varied further by implementing two grid discretisation, i.e., a coarse grid and a finer computational grid. The results of these various models are evaluated by comparing the model output to wave data measured along Belgian coastal measuring stations using calculated statistical parameters. In addition, the spectral parameters are compared to measured wave spectra for two arbitrary storm events. In order to analyse the accuracy of the SWAN models in terms of the calculated long-term extreme values (LTEVA), the SWAN models (calibrated/uncalibrated forced with ECMWF-ERA5 and DOWA) are run over an eight-year period on a coarse and fine numerical grid. The calculated LTEVA for the measured values is compared with the calculated LTEVA of each SWAN model and with published values.

The final section of this study investigates whether nested grids (three nested grids at a reduction scale of 1:5) have an impact on the model results when considering the calibrated and uncalibrated SWAN models forced with the ECMWF-ERA5 and DOWA wind databases. The model results are compared to measured data along the Belgian coast.

### 3.2. Wind Hindcast Databases

Wind hindcast databases are used as input to force the SWAN numerical wave model in order to produce wave parameters as output. The hindcast near-surface wind datasets used in the numerical modelling originates from the ECMWF-ERA5 wind database ([23,24]) and the DOWA database ([25–27]).

#### 3.2.1. ECMWF-ERA5 Reanalysis

Global long-term hindcast wind data and forecast data (from 1979 to present) are primarily available from the ECMWF-ERA5 database developed through the Copernicus Climate Change Service (C3S) and available from the Copernicus Data Store [23]. The ECMWF-ERA5 dataset is a combination of modelled and observed values, calculated using 4D-Var data assimilation techniques via the ECMWF Integrated Forecast System (IFS), cycle 41r2 ([24,28]). The ECMWF-ERA5 database publishes atmospheric data on an hourly temporal scale and on a  $0.25^\circ \times 0.25^\circ$  spatial scale.

#### 3.2.2. Dutch Offshore Wind Atlas (DOWA)

Wind data from the DOWA database was released in 2018. The DOWA aims to improve on the KNW-atlas through better representation and correlation of the diurnal cycle. The wind atlas generates realistic three-dimensional wind fields and incorporates meteorological measurements recorded between 2008 and 2017. The forecasting model HARMONIE/AROME [29] has been used by KNMI since 2012, to downscale the DOWA to a horizontal grid of 2.5 km. Innovative measurements, not used by ECMWF-ERA5, are assimilated into the DOWA thereby adding realistic detail to the wind speeds and directions ([25,26]). Duncan et al. ([25,26]) validated the DOWA modelled wind speeds and directions with offshore and nearshore LiDAR, wind-mast measurements and ASCAT satellite observations for the year 2013. The authors found that the DOWA compared very well to the measurements. It is reported by the authors that the DOWA did not improve the relative error of the average wind speeds at 10 m above MSL when compared to ASCAT measurements and to the ECMWF-ERA5 data. In addition, ref. [25] reports that the DOWA, on average, overestimates the average wind speeds at 10 m heights while ECMWF-ERA5 shows almost zero bias. However, the DOWA did show an improved

correlation to measurements and better capture of the small-scale structures in the wind fields. Note, however, that most of the comparisons were made for winds at 90 m heights above MSL as opposed to 10 m above MSL used as input for wave models.

### 3.3. Buoy Measured Wave Data

Measured wave data from various stations throughout the Belgian continental shelf were obtained from the Flemish Agency for Maritime Services and Coast (MDK) for the analysis period [30]. The data at the various points were measured with waverider buoys. For some stations only non-directional data is available. The data is validated internally by the data controllers at MDK. Live and historical data is also available online from the Vlaamse Meetnet Banken portal. The wave data measurement locations are shown in Figure 2.

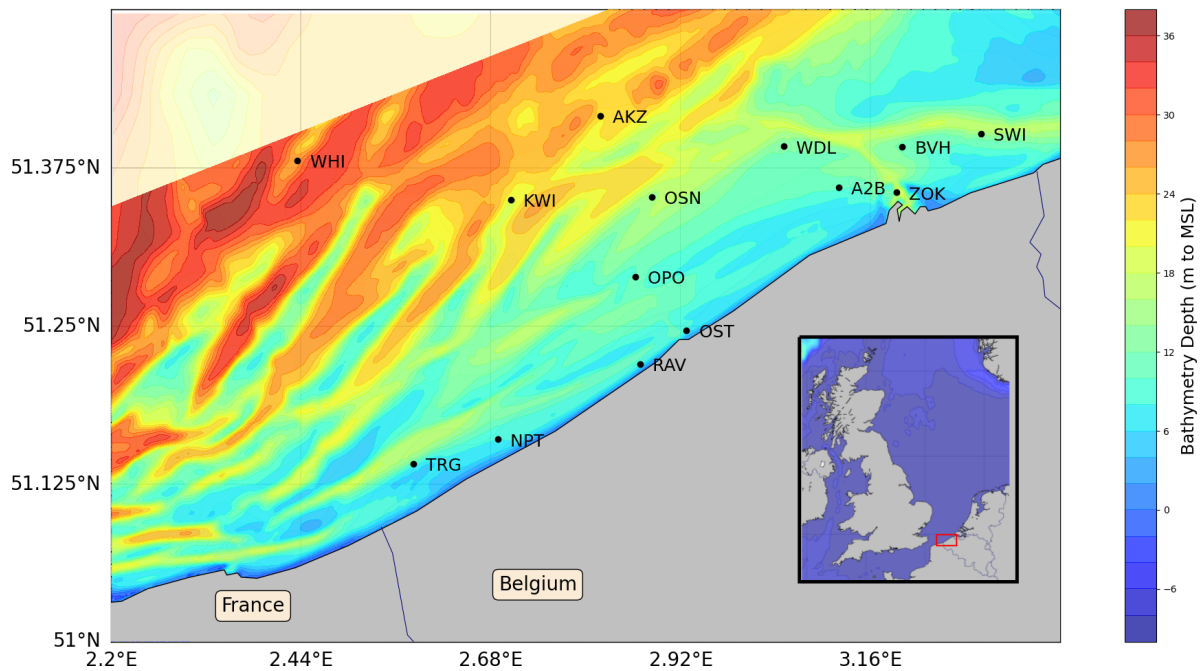


Figure 2. Map of observation stations located throughout the Belgian Continental Shelf.

### 3.4. Numerical Formulation of SWAN

The SWAN software solves the action balance equation, where the rate of change of the action density  $N(x, y, t, \sigma, \theta)$  at a particular point in space, is given as follows ([4,31]):

$$\frac{\partial N}{\partial t} + \nabla_{x,y} \cdot [(\bar{c}_g + \bar{U})N] + \frac{\partial c_\sigma N}{\partial \sigma} + \frac{\partial c_\theta N}{\partial \theta} = \frac{S_{tot}}{\sigma} \quad (1)$$

where:

- $\nabla_{x,y} \cdot [(\bar{c}_g + \bar{U})N]$  denotes the wave energy propagation (which includes wave shoaling) where:
  - $\bar{c}_g$  is the group velocity; and
  - $\sigma^2 = g|\bar{k}| \tanh(|\bar{k}|d)$  follows from the dispersion relation where  $\bar{k}$  is the wave number vector and  $d$  the water depth
- $\frac{\partial c_\sigma N}{\partial \sigma}$  is the term that shifts the radian frequency due to depth and current induced diffraction;
- $\frac{\partial c_\theta N}{\partial \theta}$  represents refraction due to currents and bathymetry changes where the propagation velocities in spectral space  $(\sigma, \theta)$  are represented by  $c_\sigma$  and  $c_\theta$ ; and
- $\frac{S_{tot}}{\sigma}$  contains the non-conservative terms that represent the sink/source terms (e.g., wind growth, etc.) that redistributes, generates or dissipates energy at a point in space.

The non-conservative terms that contribute to  $S_{tot}$  within the SWAN model are:

- $S_{in}$ : wave growth by wind (energy generation);
- $S_{nl3}$ : three wave energy transfer (redistribution of energy);
- $S_{nl4}$ : four wave energy transfer (redistribution of energy);
- $S_{ds,w}$ : white capping (energy dissipation);
- $S_{ds,b}$ : bottom friction (energy dissipation); and
- $S_{ds,br}$ : depth limited wave breaking (energy dissipation).

### 3.5. Wind Formulation in SWAN: $S_{in}$

Contribution to the source terms by  $S_{in}$  in SWAN is calculated using the wave resonance method (Phillips, 1957) [32] and the wave feedback method (Miles, 1957) [33]. As such, wave growth is calculated in SWAN as the sum of a linear ( $A$ ) and an exponential ( $BE(\sigma, \theta)$ ) growth term of a wave component as follows:

$$S_{in}(\sigma, \theta) = A + BE(\sigma, \theta) \tag{2}$$

where  $A$  and  $B$  depend on the wave and wind frequencies ( $\sigma$ ) and directions ( $\theta$ ). The input wind vector,  $\bar{u}_{10}$ , is assumed to be at 10 m height above reference level and translated to a friction velocity  $\bar{u}_*$  and the drag coefficient  $C_D$  computed, as follows:

$$\begin{aligned} \bar{u}_*^2 &= C_D \bar{u}_{10}^2, \\ C_D(\bar{u}_{10}) &= (0.55 + 2.97\bar{u} - 1.49\bar{u}^2) / 1000, \\ \bar{u} &= \frac{\bar{u}_{10}}{u_{ref}} = \frac{\bar{u}_{10}}{31.5 \text{ m/s}} \end{aligned} \tag{3}$$

as detailed in Zijlema et al. (2012) [34] where the authors fitted a weighted best-fit second order polynomial to observed values of the wind drag coefficient from various published studies. The reference value  $u_{ref} = 31.5 \text{ m/s}$  is the wind speed where the drag coefficient is a maximum from the polynomial fit.

SWAN uses the formulation of Phillips for the initial linear wave growth calculation and the formulation based on Miles to calculate the feedback wind-wave growth.

#### 3.5.1. Linear (Initial) Wave Growth Component

The linear component ( $A$ ) of the wind wave source term is based on the assumption of Phillips [32] that for a constant wind, the transfer from the air-pressure waves to the sea surface gravity waves by resonance, is constant in time, therefore leading to linear growth in time (Equation (2)). The linear component is calculated using the formulation of Cavaleri and Malanotte-Rizzoli (1981) [35] where initial waves are imposed on the model using their empirical formulation:

$$S_{in,l}(f, \theta) = \begin{cases} C_\alpha [\bar{u}_* \cos(\theta - \theta_{wind})]^4 & \text{for } |\theta - \theta_{wind}| \leq 90^\circ \text{ and } f \geq f_{PM} \\ 0 & \text{for all other wave components} \end{cases} \tag{4}$$

where  $C_\alpha = \frac{1.5 \times 10^{-3}}{2\pi g^2}$  and  $\theta_{wind}$  is the wind direction and  $f_{PM}$  is the Pierson–Moskowitz peak frequency. Note that  $S_{in,l}(f, \theta)$  is only valid for initial wave growth as this source term is much smaller than the wind-wave source term contribution  $S_{in}(f, \theta)$ .

Tolman [36] added a low frequency filter to Equation (4). He argued that, at the initial point of wave generation, wave growth takes place at high frequencies. However, the model is calculated on a discrete frequency grid where dependence on the low-frequency extent of the frequency discretization could lead to artificial initial wave growth. As such,

mean wave parameters are not influenced at initial growth. The equation then takes the form of:

$$S_{in,l}(f, \theta) = C_\alpha [\bar{u}_* \max[0, \cos(\theta - \theta_{wind})]]^4 \times \exp \left[ - \left( \frac{f}{f_{PM}} \right)^{-4} \right] \tag{5}$$

$$f_{PM} = \frac{2\pi \times 0.13g}{28\bar{u}_*}$$

Equation (5) is implemented in SWAN to compute the initial linear growth of the wind-waves; however, this linear term must be explicitly activated in SWAN.

### 3.5.2. Exponential Component

Two expressions for the calculation of the exponential component  $B$  are available in SWAN:

**Komen et al. (1984) [21]** The authors formulated the wind growth source term as a function of the phase speed  $c_{ph}$  as follows:

$$B = \max \left[ 0, 0.25\epsilon \left( \frac{28\bar{u}_*}{c_{ph}} \cos(\theta - \theta_{wind}) - 1 \right) \right] \sigma \tag{6}$$

where  $\epsilon = \rho_a / \rho_w$  with  $\rho_a$  the density of the air and  $\rho_w$  the density of the water.

**Janssen (2004) [9]** Janssen formulates the exponential term,  $S_{in} = BE(\sigma, \theta)$  according to his quasi-linear wind-wave theory derived from Miles' scaling arguments [33]. First, the wind profile is assumed

$$\bar{u}_0(z) = \frac{\bar{u}_*}{\kappa} \ln \left( \frac{z + z_1}{z_0 + z_1} \right) \tag{7}$$

where the momentum loss by air processes are represented by a background roughness length and is given by a Charnock-like relation  $z_0 = \alpha_c \bar{u}_*^2 / g$  and  $z_1$  the roughness length representing the effect of gravity waves on the wind profile.  $\kappa = 0.41$  is the Von Karman constant. Janssen notes that the determination of  $\alpha_c = 0.01$  is not so trivial due to the fact that the ratio of  $\bar{\tau}_w / \bar{\tau}$  is not known. As such, the wave models were run iteratively with the value of  $\alpha_c = 0.01$  as recommended [9].

Let  $z_2 = z_0 + z_1$  represent the effective surface roughness which can be expressed in terms of the wave-induced stress  $\bar{\tau}_w$  and the total surface stress  $\bar{\tau}$  as:

$$z_2 = \frac{z_0}{\sqrt{1 - \frac{|\bar{\tau}_w|}{|\bar{\tau}|}}} \tag{8}$$

where, assuming that the wave momentum is given by  $\bar{P} = \bar{k}E(\sigma, \theta)$ , the wave-induced stress is given by

$$\begin{aligned} \bar{\tau}_w(z = 0) &= \int \partial\sigma \partial\theta \bar{k} \frac{d}{dt} E(\sigma, \theta)_{wind} \\ &= \rho_w \int_0^{2\pi} \int_0^\infty \sigma BE(\sigma, \theta) \frac{\bar{k}}{k} d\sigma d\theta \end{aligned} \tag{9}$$

and the total stress by

$$\bar{\tau} = \rho_a |\bar{u}_*| \bar{u}_* \tag{10}$$

The exponential term  $B = \epsilon\omega\beta x^2$  is then calculated as given in Appendix A (Equation (A5)) where  $\beta_m = 1.2$  (Equation (A4)) was chosen so that the growth rate agrees with the numerical results obtained by Miles' theory and with observations.

### 3.6. Wave Dissipation Dynamics: White Capping: $S_{ds,w}$

White capping is one of the least understood processes represented in numerical models. Strictly speaking, the physics of energy loss due to white capping is linked to the wind-wave growth/dissipation as white capping is directly related to the momentum transfer of the wind-wave energy in an active sea [10]. SWAN utilises the white capping formulation proposed by Komen et al. (1984) [21] where the energy dissipation is modelled using the spectral mean wave steepness. Using the average wave steepness across a wave spectrum, which includes wind- and swell-seas, introduces the problem that the dissipation rate is too high for the swell part and too little for the wind part of the spectrum. The proposed source term ( $S_{ds,w}$ ) formulation by Komen et al. is based on the pulse-based model proposed by Hasselmann (1974) [37], reformulated by the WAMDI group (1988) [38] to be applicable to shallow water and adjusted by Günther et al. (1992) [39] as follows:

$$S_{ds,w}(\sigma, \theta) = -\Gamma \bar{\sigma} \frac{k}{\bar{k}} E(\sigma, \theta), \text{ where} \tag{11}$$

$$\Gamma = C_{ds} \left( (1 - \delta) + \delta \frac{k}{\bar{k}} \right) \left( \frac{\bar{s}}{\bar{s}_{PM}} \right)^p$$

$$\bar{s} = \bar{k} \sqrt{E_{tot}}$$

and  $\bar{s}$  is the total wave steepness with  $\bar{s}_{PM} = \sqrt{3.02 \times 10^{-3}}$  the value of the wave steepness in the Pierson–Moskowitz spectrum. The calculation of  $\bar{\sigma} \bar{k}$  and  $E_{tot}$  is as defined by the WAMDI Group [38]. The parameters defined by the white capping coefficient,  $C_{ds}$ ,  $\delta$  and  $p$  are coefficients intended to tune the numerical model for a given modelling scenario [31].

Two sets of coefficients have been determined by Komen et al. (1984) and Janssen (1992) by assuming idealised growth conditions and closing the energy balance of the waves. The coefficients are summarised in Table 2.

**Table 2.** White capping coefficients as determined by Komen et al. (1984) and Janssen (1992).

	$C_{ds}$	$\delta$	$p$
Komen et al. (1984) [21]	$2.36 \times 10^{-5}$	0	4
Janssen (1992) [22]	$4.10 \times 10^{-5}$	0.5	4

Van der Westhuysen (2007) [40] proposed an alternative white capping formulation used in conjunction with the wind formulation of Yan (1987) [41] and is an option for wind-wave growth in SWAN. The advantage of the Komen/Janssen formulations is that the wind-wave growth of either formulations can be used interchangeably with the white capping formulations whereas Van der Westhuysen and Yan are inseparable and cannot be combined with Komen or Janssen formulations [31].

### 3.7. Computational Domain

The computational grid is an important part of the model design. For instance, the wind input forcing dataset has a spatial discretisation that could be finely- or coarsely defined relative to the SWAN model computational grid. Typically, a bilinear interpolation function is used to spatially map the given input wind grid to the computational grid [31] in SWAN. As such, when the wind data is spatially coarsely distributed (relative to the computational grid in the spatial domain), it can be safely assumed that no new, smaller scale, structural wind information will be added due to the interpolation. Conversely, a spatially dense wind forcing database that is interpolated onto a coarser computational grid, might lead to a significant loss in the smaller scale wind information that was originally contained in the denser wind grid. The ECMWF-ERA5 database is supplied on an approximate  $5 \text{ km} \times 5 \text{ km}$  spatial scale while the DOWA database is output on an approximate  $2.5 \text{ km} \times 2.5 \text{ km}$  spatial scale; i.e., mapping the DOWA wind to a  $5 \text{ km} \times 5 \text{ km}$  computational grid in SWAN possibly might result in a loss of wind information.

Cavaleri et al. (2018) [10] advises that the wave model computational grid should be “sufficiently fine” for accurate results and the optimal manner is through grid nesting at a maximum of  $\rho_5$  (1:5 reduction in scale), in their experience. A sufficiently fine grid is a relative term that points to the obvious difficulty that finer grid cells are needed where wave conditions cause high gradients, which cannot be determined a priori.

For this study, three SWAN computational grid resolutions of approximately  $2.5 \text{ km} \times 2.5 \text{ km}$ ,  $5 \text{ km} \times 5 \text{ km}$  and  $7.5 \text{ km} \times 7.5 \text{ km}$  are used. The definition of grids is shown graphically in Figure 3.

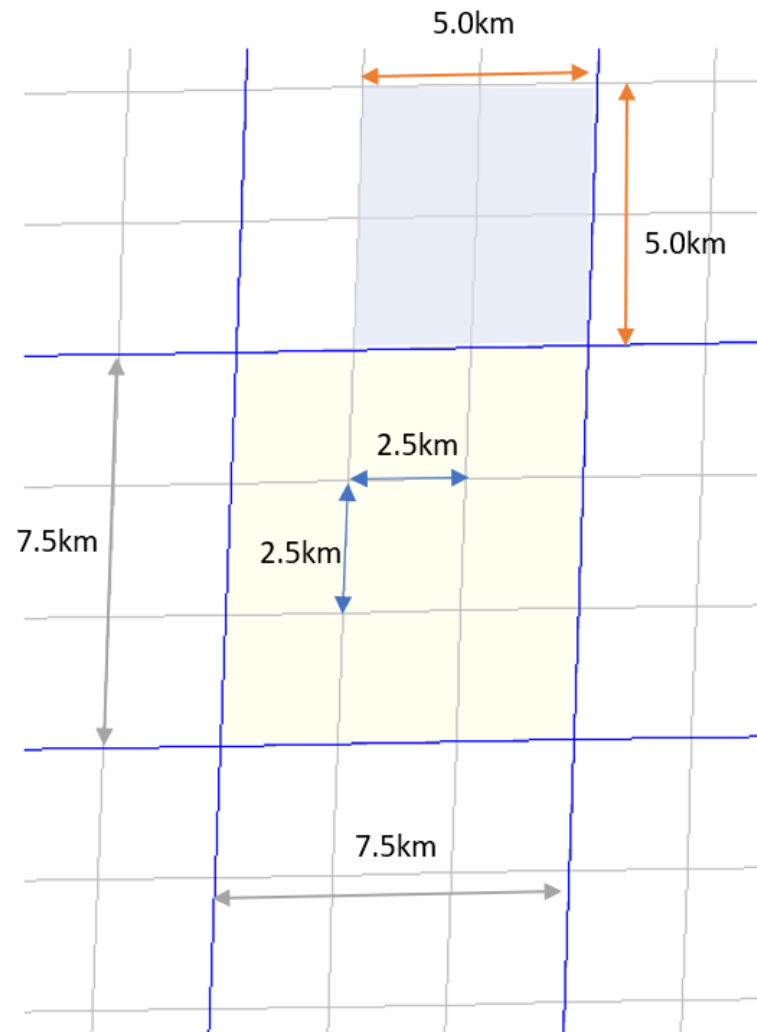


**Figure 3.** SWAN model grid discretisation for the dense (approx 2.5 km), medium (approximately 5 km) and coarse (7.5 km) computational grids.

### 3.8. Bathymetry

Various sources of bathymetric data were used in the model setup. Measurements at 84,252 points over an area of  $5625 \text{ km}^2$ , including a large amount of LiDAR data for Belgian beaches, collected from various measuring campaigns from 2009 to 2013, were provided by MDK for this study. External data from the Etopo2 global database were used to define the offshore regions. The bathymetric data used are expressed with respect to Mean Sea Level (MSL). Note that the modelled water depths for the various stations are as follows: AKZ 22.6 m; KWI 21.3 m; OSN 16.8 m; SWI 11.8 m; TRG 9.6 m; WDL 13.7 m; WHI 29.6 m with depth relative to MSL.

### 3.9. SWAN Model Settings

For the most part, the SWAN model settings are determined by the specific modelling campaign. However, as mainly the wind and white capping parameters are investigated in this study, the following model settings representing the model physics (Table 3) and numerical parameters (Table 4) are kept consistently throughout this study:

**Table 3.** Physical parameters used in the SWAN model setup.

Wind formulation and White capping	The third generation model of SWAN is used. The wind-wave and white capping formulation varies with modelling campaign
Quadruplets	The default option is selected: “Fully explicit computation of the nonlinear transfer with DIA per sweep” [31]
Wave Breaking	The formulation of Battjes and Janssen [42] with $\alpha = 1.0$ and $\gamma = 0.78$ is used
Bottom friction	The JONSWAP coefficient of $0.038 \text{ m}^2/\text{s}^3$ is applied as a constant over the domain following [34]
Triads	The default value for Triads are used, i.e., the LTA method of Eldeberky (1996) [43]
Limiter	The default limiter values are used, i.e., Ursell upper threshold = 10 and the fraction for breaking waves = 1.0
Vegetation, Mud, Obstacles, Setup and Turbulence	These options are not activated as these processes are not relevant on this scale
Diffraction	The activation if diffraction is irrelevant in this study

**Table 4.** Numerical parameters used in the SWAN model setup.

Propagation	The BSBT Scheme is used,
Numerical parameters	The default numerical parameters are used.
Iteration Stop Criteria	The iteration stop criteria is set at 2% and run in non-stationary mode.

### 3.10. Computer Hardware

The model runs were conducted on a dual processor machine ( $2 \times$  Intel Xeon Gold 6140 2.3 G) with a total of 18 cores (36 threads) per processor and a total of 64 Gb of memory on a Linux Mint LMDE3 platform.

## 4. Results

### 4.1. Model 1: Calibrated vs. Uncalibrated SWAN Model

#### 4.1.1. Visual Comparison

The significant wave heights, peak spectral period and spectral peak wave directions for the calibrated and uncalibrated models are compared to measured wave data for a number of stations along the Belgian coastline. Figures 4 and 5 are time series plots showing model results for both the ECMWF-ERA5 and DOWA wind databases, respectively, at the Kwintebank measuring station which show that the SWAN models appear to have a good visual correlation with the measured data.

#### 4.1.2. Statistical Analysis: Significant Wave Height

The statistical accuracy (see Appendix B for the definition of the formulas used) for the calibrated and uncalibrated models forced by the ECMWF-ERA5 and DOWA wind databases, modelled on a  $5.0 \text{ km} \times 5.0 \text{ km}$  grid, are given in Tables 5 and 6, respectively. The statistical comparisons, for the calibrated and uncalibrated SWAN models on a  $2.5 \text{ km} \times 2.5 \text{ km}$  grid, are shown in Tables 7 and 8 forced by the ECMWF-ERA5 and DOWA databases, respectively.

In each model, the relevant wind database is interpolated onto both the coarse and finer SWAN computational grids (Section 3.7).

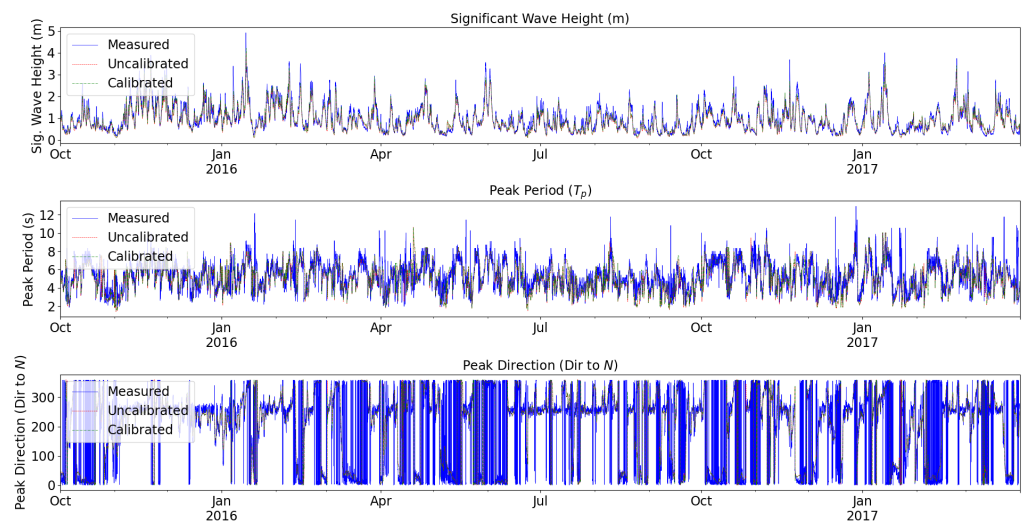


**Figure 4.** Significant wave height (**top** panel), peak period (**centre** panel) and peak wave direction (**bottom** panel) time series plots for the ECMWF-ERA5 forced SWAN model showing the measured data vs. the uncalibrated SWAN model and calibrated SWAN model for the Kwintebank station.

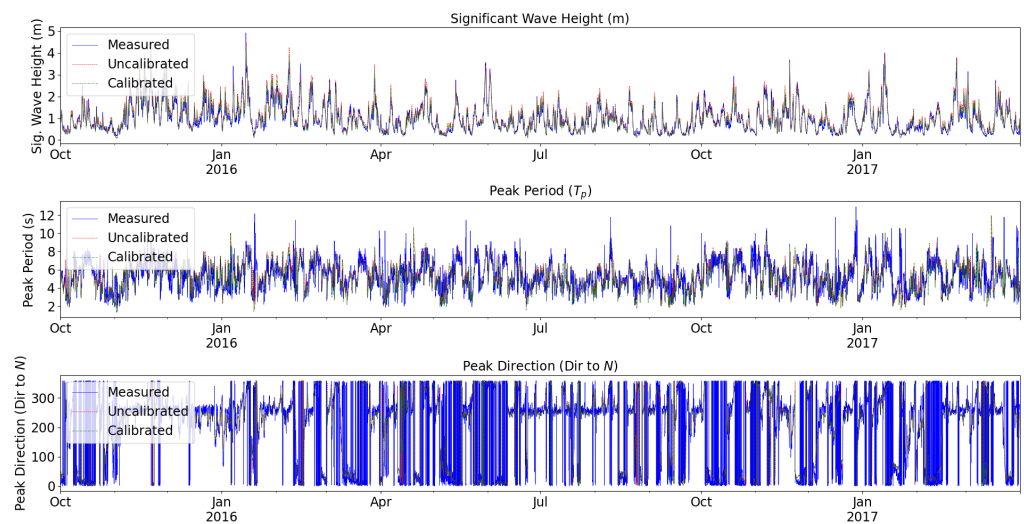


**Figure 5.** Significant wave height (**top** panel), peak period (**centre** panel) and peak wave direction (**bottom** panel) time series plots for the DOWA forced SWAN model showing the measured data vs. the uncalibrated SWAN model and calibrated SWAN model for the Kwintebank station.

**Table 5.** Significant wave height statistical parameters calculated for the calibrated and uncalibrated SWAN models, 5.0 km × 5.0 km computational grid, forced by the ECMWF-ERA5 database.

Station	ECMWF-ERA5			Mean (m)			SD (m)			Bias (m)		RMSE (m)		Corr Coeff (-)	
	Mea-sured	Uncali-brated	Cali-brated	Mea-sured	Uncali-brated	Cali-brated									
AKZ	1.03	0.93	0.98	0.63	0.56	0.58	0.10	0.05	0.23	0.20	0.95	0.95			
KWI	1.00	0.89	0.95	0.61	0.54	0.56	0.10	0.05	0.22	0.19	0.95	0.95			
OSN	0.93	0.84	0.88	0.58	0.51	0.53	0.09	0.04	0.21	0.18	0.95	0.95			
SWI	0.54	0.64	0.68	0.35	0.40	0.42	-0.10	-0.13	0.16	0.16	0.70	0.70			
TRG	0.58	0.60	0.63	0.41	0.36	0.38	-0.02	-0.05	0.17	0.17	0.91	0.91			
WDL	0.75	0.81	0.85	0.49	0.49	0.51	-0.06	-0.10	0.17	0.17	0.82	0.82			
WHI	1.11	0.96	1.01	0.69	0.57	0.59	0.16	0.10	0.28	0.24	0.91	0.91			

**Table 6.** Significant wave height statistical parameters calculated for the calibrated and uncalibrated SWAN models, 5.0 km × 5.0 km computational grid, forced by the DOWA database.

DOWA	Mean (m)			SD (m)			Bias (m)		RMSE (m)		Corr Coeff (-)	
Station	Mea-sured	Uncali-brated	Cali-brated	Mea-sured	Uncali-brated	Cali-brated	Uncali-brated	Cali-brated	Uncali-brated	Cali-brated	Uncali-brated	Cali-brated
AKZ	1.03	1.12	1.01	0.63	0.68	0.63	-0.09	0.02	0.23	0.19	0.95	0.95
KWI	1.00	1.10	0.99	0.61	0.67	0.61	-0.10	0.00	0.21	0.17	0.96	0.96
OSN	0.93	1.02	0.92	0.58	0.63	0.58	-0.10	0.00	0.20	0.16	0.96	0.96
SWI	0.54	0.80	0.72	0.35	0.51	0.48	-0.17	-0.10	0.24	0.17	0.71	0.71
TRG	0.58	0.76	0.69	0.41	0.47	0.44	-0.18	-0.11	0.25	0.20	0.93	0.93
WDL	0.75	0.99	0.89	0.49	0.61	0.56	-0.17	-0.08	0.25	0.18	0.83	0.83
WHI	1.11	1.18	1.07	0.69	0.72	0.66	-0.06	0.05	0.20	0.19	0.91	0.92

**Table 7.** Significant wave height statistical parameters calculated for the calibrated and uncalibrated SWAN models, 2.5 km × 2.5 km computational grid, forced by the ECMWF-ERA5 database.

ECMWF-ERA5	Mean (m)			SD (m)			Bias (m)		RMSE (m)		Corr Coeff (-)	
Station	Mea-sured	Uncali-brated	Cali-brated	Mea-sured	Uncali-brated	Cali-brated	Uncali-brated	Cali-brated	Uncali-brated	Cali-brated	Uncali-brated	Cali-brated
AKZ	1.03	0.94	1.04	0.63	0.56	0.61	0.09	-0.01	0.21	0.19	0.95	0.95
KWI	1.00	0.90	1.00	0.61	0.53	0.57	0.10	0.00	0.21	0.18	0.96	0.95
OSN	0.93	0.84	0.94	0.58	0.51	0.55	0.08	-0.01	0.20	0.18	0.95	0.95
SWI	0.54	0.64	0.71	0.35	0.39	0.42	-0.10	-0.17	0.14	0.18	0.71	0.70
TRG	0.58	0.63	0.70	0.41	0.38	0.41	-0.04	-0.11	0.17	0.20	0.91	0.91
WDL	0.75	0.81	0.89	0.49	0.49	0.53	-0.06	-0.15	0.15	0.18	0.82	0.82
WHI	1.11	0.97	1.07	0.69	0.57	0.62	0.14	0.04	0.27	0.21	0.91	0.91

**Table 8.** Significant wave height statistical parameters calculated for the calibrated and uncalibrated SWAN models, 2.5 km × 2.5 km computational grid, forced by the DOWA database.

DOWA	Mean (m)			SD (m)			Bias (m)		RMSE (m)		Corr Coeff (-)	
Station	Mea-sured	Uncali-brated	Cali-brated	Mea-sured	Uncali-brated	Cali-brated	Uncali-brated	Cali-brated	Uncali-brated	Cali-brated	Uncali-brated	Cali-brated
AKZ	1.03	1.14	1.02	0.63	0.69	0.63	-0.11	0.01	0.24	0.19	0.95	0.95
KWI	1.00	1.10	0.99	0.61	0.66	0.61	-0.11	0.01	0.21	0.17	0.96	0.96
OSN	0.93	1.03	0.92	0.58	0.62	0.57	-0.10	0.00	0.20	0.16	0.96	0.96
SWI	0.54	0.79	0.71	0.35	0.50	0.46	-0.25	-0.17	0.23	0.16	0.72	0.72
TRG	0.58	0.80	0.72	0.41	0.49	0.46	-0.21	-0.13	0.28	0.22	0.93	0.93
WDL	0.75	0.99	0.88	0.49	0.61	0.55	-0.24	-0.14	0.25	0.17	0.83	0.83
WHI	1.11	1.20	1.07	0.69	0.73	0.67	-0.09	0.03	0.20	0.19	0.92	0.91

Considering the 5.0 km × 5.0 km grid resolution SWAN model results shown in Tables 5 and 6, it can be observed that the bias for the uncalibrated SWAN model forced with DOWA skews towards the modelled values in the order of 5 cm to 18 cm in all stations. Both the calibrated SWAN models (forced with ECMWF-ERA5 and DOWA) and the uncalibrated model forced with ECMWF-ERA5 are, for all stations except Westhinder (WHI), biased between 5 cm and 13 cm. Considering the same dataset, the mean wave height is underestimated for stations AKZ, KWI, OSN and WHI and overestimated for stations SWI, TRG and WDL. The uncalibrated DOWA forced SWAN model consistently calculates a higher mean significant wave height compared to the measured values.

The calculated RMSE for all models and all stations, lie between 15 cm and 28 cm. In particular, it can be seen that the calibrated SWAN model forced with ECMWF-ERA5 improves the RMSE, in general, by approximately 4 cm while the calibrated DOWA forced SWAN model improves the RMSE, in general, in the order of 4 cm to 7 cm. The calibrated SWAN model forced with DOWA has a lower RMSE in the order of 1 cm to 5 cm relative to the calibrated ECMWF-ERA5 forced SWAN model.

Comparing the effect of the grid resolution, i.e., Table 5 with Table 7 (5 km coarser grid vs. 2.5 km fine grid for the SWAN model forced with ECMWF-ERA5) and Table 6 with

Table 8 (5 km coarser grid vs. 2.5 km fine grid for the DOWA forced SWAN model), no clear improvement in the metrics from large grid to smaller grid are observed. In general, the metrics are within 1 cm–3 cm of each other and a marginal improvement of the calibrated models (mean significant wave height and RMSE) are seen by reducing the resolution of the SWAN computational grid to 2.5 km × 2.5 km.

Comparing the ECMWF-ERA5 forced SWAN wind-wave model statistical results with that of the SWAN model forced with the DOWA wind database, the results show small differences in all statistical parameters when considering the varied grid sizes and the calibration status of each of the models. The largest differences in the RMSE metric are observed between the uncalibrated models (e.g., stations WDL and WHI) in the order of 7 cm to 10 cm (Tables 5–8). For the calibrated models, the largest difference of 5 cm in RMSE is seen at station WHI for the 5.0 km grids whereas the improvement of RMSE in the finer (2.5 km) grid is in the order of 2 cm at station TRG.

The RMSE is significant in terms of the average wave heights. This indicates that an RMSE of, say 20 cm, with an average wave height of 1.0 m implies a 20% error on the part of the model. In particular, the DOWA forced uncalibrated SWAN model seems to result in higher RMSE values for stations with lower average wave heights. This implies that the relative modelled error increases for these stations, e.g., for station SWI, where the measured average wave height is 54 cm and the RMSE for the uncalibrated model is 24 cm, implies a significant error, in the order of 44% of the measured average wave height and for station WHI, where the measured average wave height is 1.11 m and the RMSE for the uncalibrated model is 20 cm, implies an error in the order of 18% of the measured average wave height.

#### 4.1.3. Wave Direction

The influence of the grid size on the model results relative to the measured data (in terms of peak wave direction) is shown for the Westhinder station in Figures 6 and 7.

Considering the modelled wave direction results, no significant difference can be seen between the calibrated and uncalibrated SWAN model results forced with the ECMWF-ERA5 and DOWA databases, nor any differences in the models run with the coarse (5 km) and finer (2.5 km) computational grids. In fact, both the ECMWF-ERA5 and DOWA forced SWAN models show the same dominant wind trend from the south-westerly sector.

In contrast, the measured wave directions show a significant dominant north north-eastern component which is not present in the modelled results. The measured data show an almost even split between westerly and west-south westerly waves whereas the modelled waves only emphasise the west-south westerly waves. This trend is observed across all wave heights for all the models, i.e., measured data reports dominant north-northeasterly waves while the modelled results show the waves to be dominant west-south westerly waves.

#### 4.1.4. Spectral Comparison

The spectral energies for two storm wave events at their peaks are spectrally analysed and the SWAN modelled (5 km computational grid) and measured data compared for the Kwintebank measuring station. Note that measured spectral data is only available for a few Belgian stations. The measured significant wave height series for these two storm events are shown in Figure 8.

Figures 9–12 show the 1D spectral energies for the measured, SWAN uncalibrated and calibrated models for the two chosen storms at Kwintebank. The calculated significant wave height for each 1D spectrum is shown in the respective figure.

The high-frequency tail and the lower spectral frequencies are well represented by the SWAN model. The SWAN models calculate the cumulative wave energy at the measured spectral frequencies well; however, the spectral peak is not well represented by the SWAN models in all modelled cases. The calibrated models have a limited influence on the spectral shape and peak. However, the calibrated models forced with the ECMWF-ERA5 database

do seem to improve the accuracy of the significant wave height while the uncalibrated SWAN model forced with the DOWA database, appears to reflect the measured significant wave height more accurately.

### Waveroses: Significant wave height (m) for station: WHI

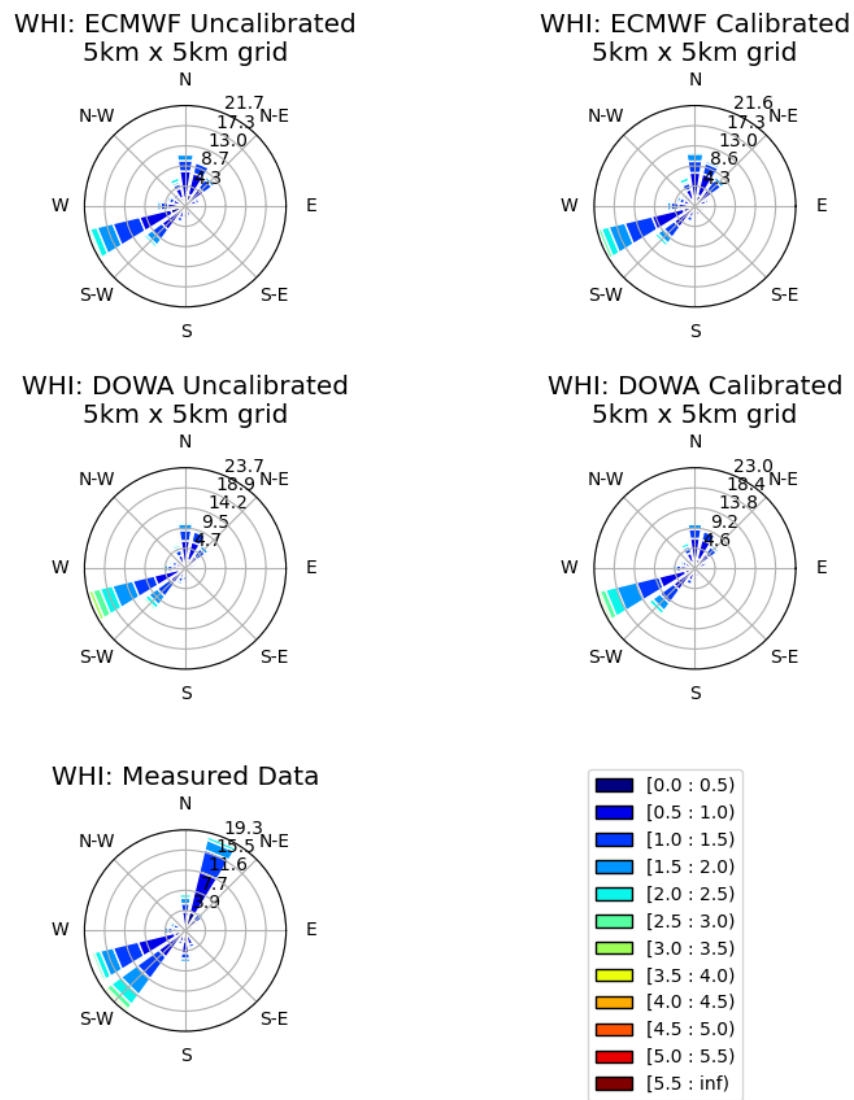


**Figure 6.** Wave roses (significant wave height) for the 5 km computational grid showing the measured data, the calibrated and uncalibrated SWAN models forced with the ECMWF-ERA5 and DOWA wind databases.

### Waveroses: Significant wave height (m) for station: WHI

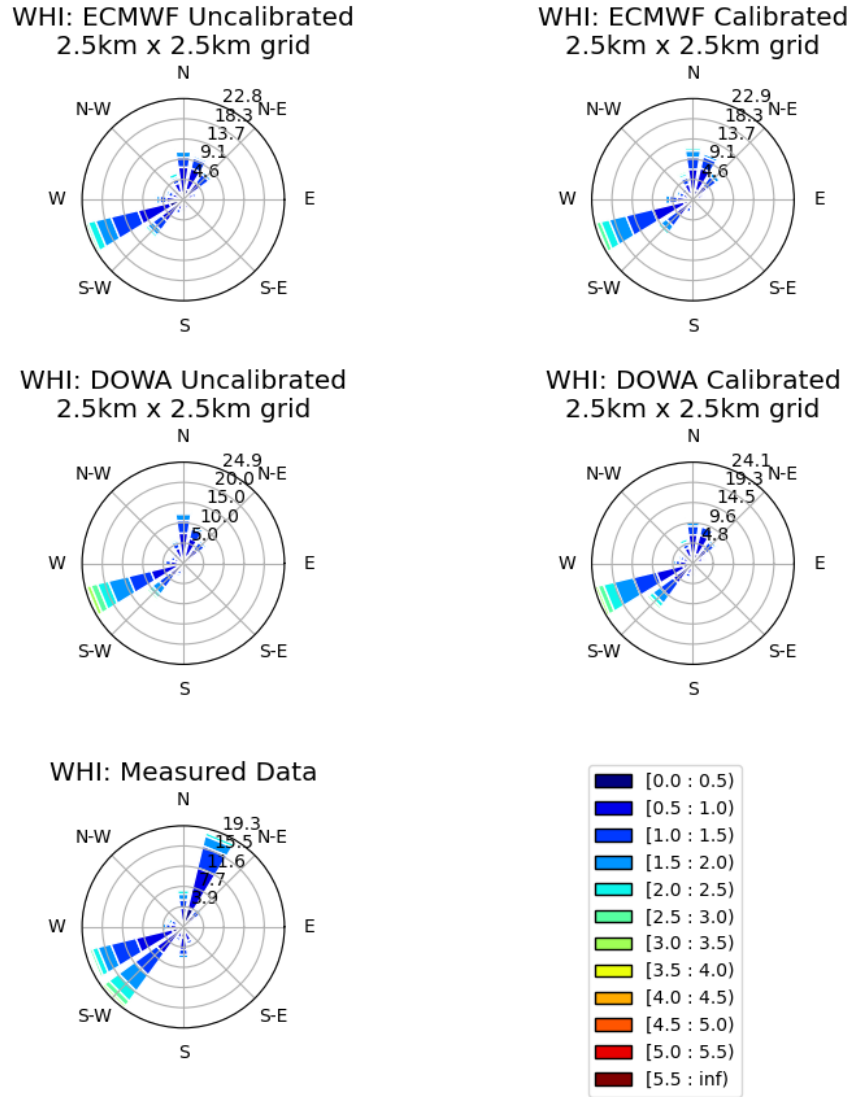


**Figure 7.** Wave roses (significant wave height) for the 2.5 km computational grid showing the measured data, the calibrated and uncalibrated SWAN models forced with the ECMWF-ERA5 and DOWA wind databases.

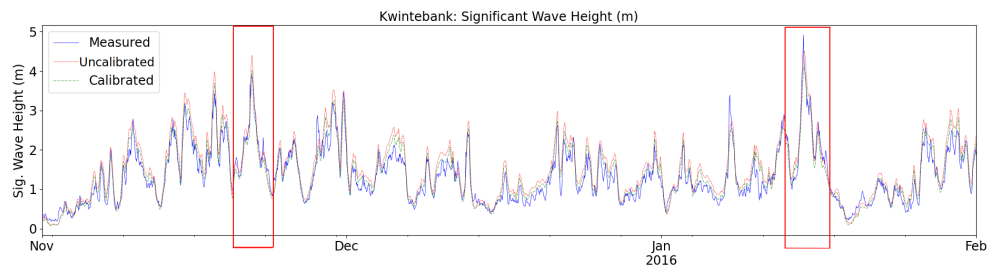


**Figure 8.** Significant wave height peaks of two storms chosen for spectral analysis at Kwintebank (forced with the DOWA wind). The storm peaks considered are at 21 November 2015 16:00 and 15 January 2016 01:00.

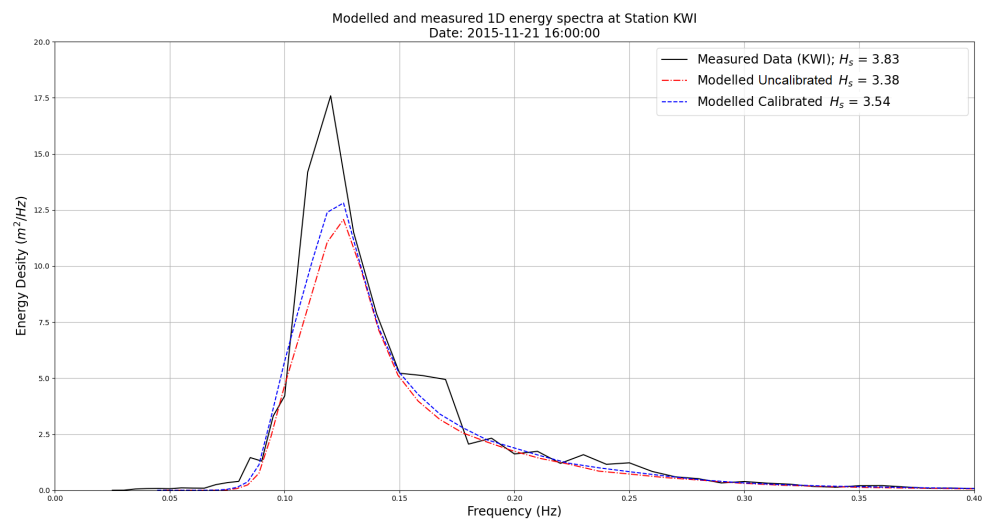


**Figure 9.** Spectral comparison for the Kwintebank station on 21 November 2015 16:00 showing the uncalibrated and calibrated SWAN models forced with ECMWF-ERA5.

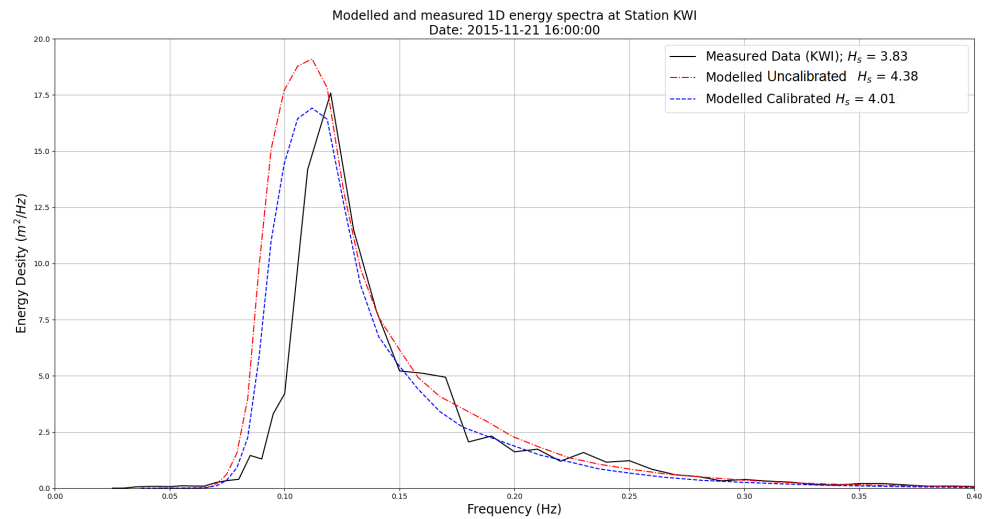


**Figure 10.** Spectral comparison for the Kwintebank station on 21 November 2015 16:00 showing the uncalibrated and calibrated SWAN models forced with DOWA.

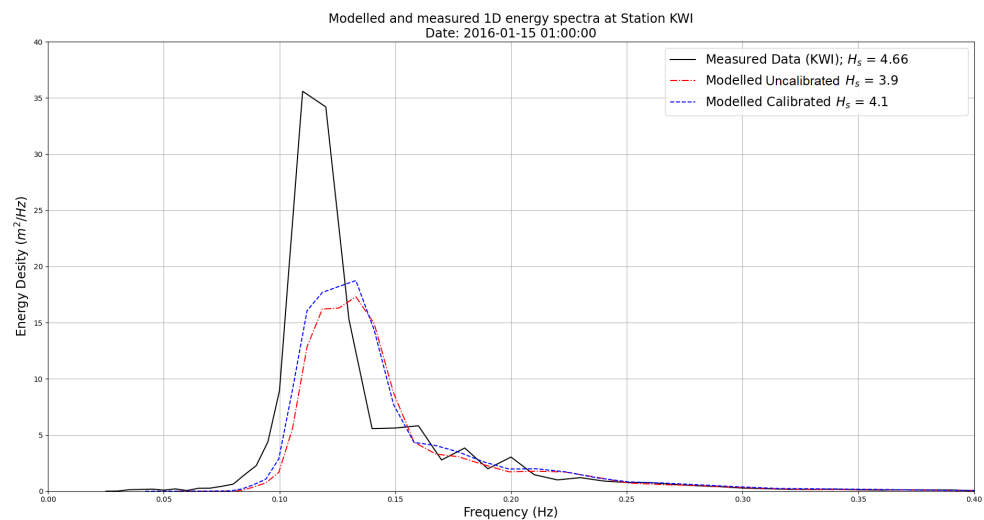


**Figure 11.** Spectral comparison for the Kwintebank station on 15 January 2016 01:00 showing the uncalibrated and calibrated SWAN models forced with ECMWF-ERA5.

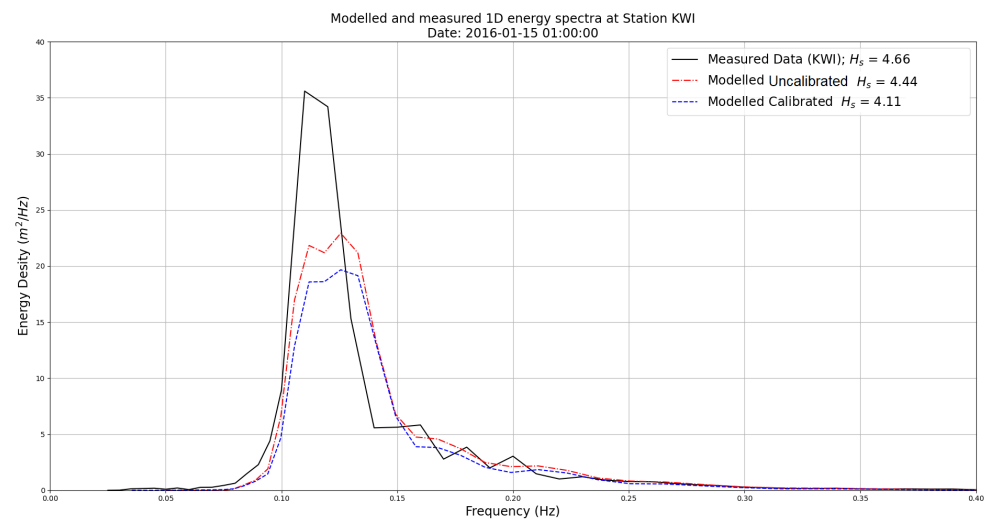


**Figure 12.** Spectral comparison for the Kwintebank station on 15 January 2016 01:00 showing the uncalibrated and calibrated SWAN models forced with DOWA.

## 4.2. Model 2: Long Term Extreme Value Analysis (LTEVA)

### 4.2.1. Introduction

This section reports on the long-term wave statistics for the period 2010 to 2017 (inclusive) by means of an Extreme Value Analysis (EVA). See Appendix C for the EVA used in this study. The measured data EVA is compared to the SWAN modelled calibrated and uncalibrated EVA for both the DOWA and ECMWF-ERA5 wind databases in order to determine the influence on calculated design parameters (e.g., the 1:100 years significant wave height). Here we compare the modelled EVA for the coarse grid (7.5 km × 7.5 km) with the EVA for the fine grid (2.5 km × 2.5 km). We investigate whether a coarse grid with a significantly faster computational time (relative to the fine grid), has any influence on the accuracy of the calculated modelled EVA when compared to measurements and published data at the same locations along the Belgian coastline.

### 4.2.2. Model Setup

The SWAN models were run with the same setup as reported in Section 3.9 for the long-term period and applied to the two computational grids (Figure 3). The modelled LTEVA is calculated from hourly significant wave height model output and compared to an EVA calculated with available measured data at hourly intervals in addition to published values [44].

### 4.2.3. Extreme Value Analysis

The extreme value analysis is performed with the `pyextremes.EVA` package in Python 3.7. [45]. The software accepts, as input, a series of significant wave heights. The following parameters are assumed and used as input into the EVA analysis:

- Method: Block Maxima
- Block window: 7 Days
- Model fit criterion (AIC) [46]: The `fit_model` method selects the best model applicable to extracted extremes using the Akaike Information Criterion (AIC)
- Continuous distributions fit to the data: Maximum Likelihood Estimate (MLE)

The `pyextremes.EVA` package returns a series of estimated extreme values for a list of given return period  $1/p$  years along with a linearised GEVA plot showing calculated significant wave height vs. return period (years). The LGEVA calculation is made for each Belgium measuring station and the SWAN modelled data for the calibrated and uncalibrated models forced with the ECMWF-ERA5 and DOWA wind databases. Extreme value plots for significant wave height against the calculated return period are presented in

Figures 13–15. The confidence interval (95%) is shown in the blue shaded upper and lower bounds. Note that only the calculated EVA graphs for the fine (2.5 km × 2.5 km) grid is shown. Note that the values from the LGEVA calculations for the calibrated and uncalibrated models forced with the ECMWF-ERA5 and DOWA wind databases, represented by the plots, are given in Tables 9 and 10 for the 2.5 km grid and 7.5 km grid, respectively, for the Westhinder station only.

The calculated long-term extreme values for a given return period are given in Table 9 for the Westhinder Station and compare the LGEVA of the measured data and the SWAN modelled data (fine grid) with published data from the Flemish Hydraulic Institute’s (Waterbouwkundig Laboratorium) published extreme value report [44]. The values in brackets indicate the percentage difference between the measured EVA values and the EVA values calculated from the SWAN models. The LGEVA of the SWAN modelled data for the 7.5 km coarse grid is given in Table 10.

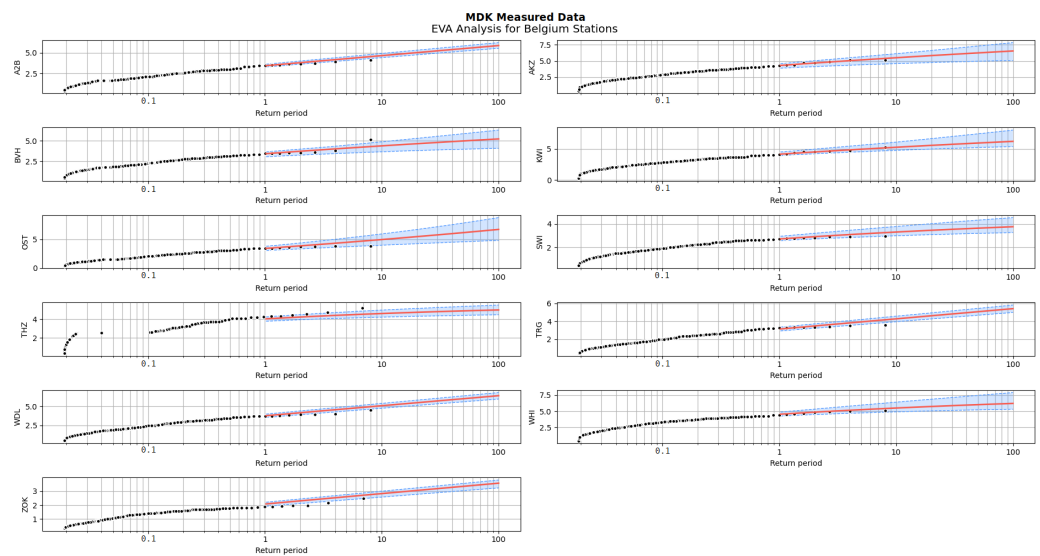


**Figure 13.** Linearised General Extreme Value Analysis plots for calculated significant wave height vs. return period (years) for measured significant wave heights at various Belgian stations.

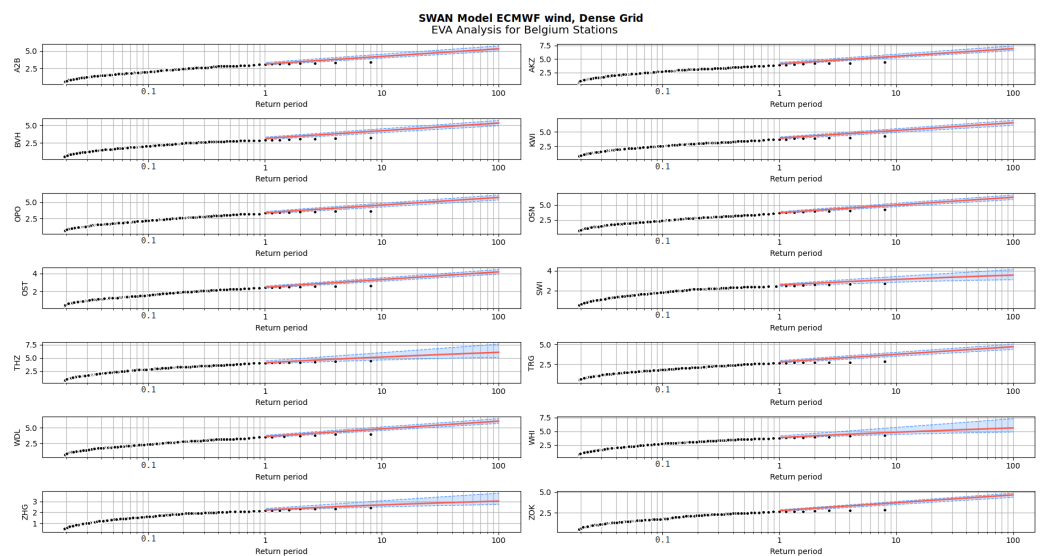


**Figure 14.** Linearised General Extreme Value Analysis plots for calculated significant wave height vs. return period (years) for the ECMWF-ERA5 forced calibrated SWAN modelled significant wave heights at various Belgian stations computed on the 2.5 km grid.

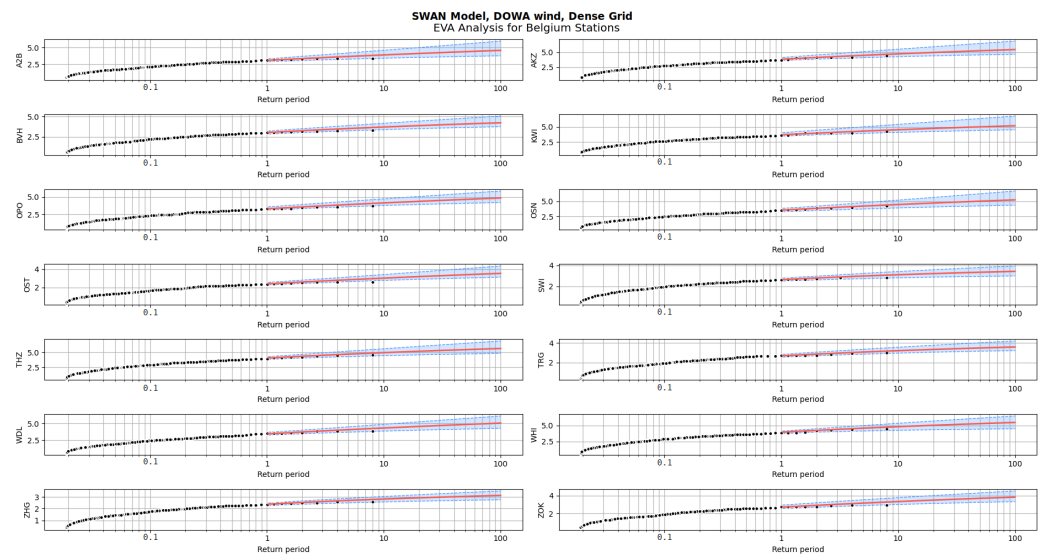


**Figure 15.** Linearised General Extreme Value Analysis plots for calculated significant wave height vs. return period (years) for the DOWA forced calibrated SWAN modelled significant wave heights at various Belgian stations computed on the 2.5 km grid.

The omni-directional significant wave height values, published in the report (for 30 min intervals) and reproduced here, are taken from a long-term analysis conducted from measurements at Westhinder and gap-filled with measurements from Akkaert-Zuid for the period between 1984 and 2019 [44]. Note that the values were read off from the omni-directional plot given in Figures 14 and 15 (directional and omni-directional return values for significant wave heights—30 min series) in the report.

**Table 9.** Calculated EVA values (and percentage difference between the measured and modelled values) from measurements and SWAN models, computed on the fine grid (2.5 km), compared to published values for deep water station at Westhinder.

Return Period	Published Values [44]	Measured Values	Calibrated SWAN Model		Uncalibrated SWAN Model	
			ECMWF-ERA5	DOWA	ECMWF-ERA5	DOWA
1	4.6 m	4.5 m	3.9 m (−14.1%)	3.9 m (−12.8%)	3.6 m (−20.7%)	4.3 m (−4.0%)
5	5.2 m	5.2 m	4.6 m (−12.4%)	4.6 m (−12.4%)	4.2 m (−20.0%)	5.0 m (−4.8%)
10	5.5 m	5.5 m	4.8 m (−11.6%)	4.8 m (−12.4%)	4.4 m (−19.6%)	5.2 m (−5.3%)
20	5.8 m	5.7 m	5.1 m (−11.0%)	5.0 m (−12.2%)	4.6 m (−19.3%)	5.4 m (−5.6%)
50	6.1 m	6.0 m	5.4 m (−10.0%)	5.3 m (−11.8%)	4.9 m (−18.9%)	5.6 m (−6.0%)
100	6.4 m	6.2 m	5.6 m (−9.2%)	5.5 m (−11.6%)	5.0 m (−18.5%)	5.8 m (−6.3%)
200	6.6 m	6.4 m	5.8 m (−8.5%)	5.6 m (−11.6%)	5.2 m (−18.3%)	6.0 m (−6.6%)

**Table 10.** Calculated EVA values (and percentage difference between the measured and modelled values) from measurements and SWAN models, computed on the coarse grid (7.5 km), compared to published values for deep water station at Westhinder.

Return Period	Published Values [44]	Measured Values	Calibrated SWAN Model		Uncalibrated SWAN Model	
			ECMWF-ERA5	DOWA	ECMWF-ERA5	DOWA
1	4.6 m	4.5 m	4.0 m (−12.9%)	4.0 m (−11.4%)	3.9 m (−15.0%)	4.5 m (0.3%)
5	5.2 m	5.2 m	4.7 m (−10.6%)	4.7 m (−10.7%)	4.6 m (−12.9%)	5.3 m (1.6%)
10	5.5 m	5.5 m	5.0 m (−9.6%)	4.9 m (−10.3%)	4.8 m (−12.0%)	5.6 m (2.1%)
20	5.8 m	5.7 m	5.2 m (−8.7%)	5.1 m (−10.1%)	5.1 m (−11.2%)	5.9 m (2.6%)
50	6.1 m	6.0 m	5.6 m (−7.3%)	5.4 m (−9.6%)	5.4 m (−10.0%)	6.2 m (3.4%)
100	6.4 m	6.2 m	5.8 m (−6.3%)	5.6 m (−9.2%)	5.6 m (−9.1%)	6.4 m (3.9%)
200	6.6 m	6.4 m	6.0 m (−5.4%)	5.8 m (−8.9%)	5.9 m (−8.3%)	6.7 m (4.4%)

From Tables 9 and 10 it can be seen that the EVA for the MDK-measured data (Section 3.3) compares very well with the published values [44]. This is to be expected as

measured data from the same source is used; clearly, there is confidence in the algorithms used in the EVA model software (pyextremes.EVA package).

All the calculated SWAN modelled EVA values for the 2.5 km fine grid are lower than the calculated EVA values from measurements. In some cases, the calculated values are between 18.3% and 20.7% lower than the published values for the ECMWF-ERA5 forced uncalibrated SWAN model calculated EVA results. The uncalibrated SWAN model forced with the DOWA dataset, showed the best correlation to the measured data calculated EVA for both the fine 2.5 km and coarse 7.5 km grids. This best model estimate for the fine grid is lower than the measured data calculated EVA by between 4.0% and 6.6%. The SWAN modelled values for the 7.5 km grid seem to be closer to the published values with the uncalibrated SWAN model forced with the DOWA dataset showing EVA significant wave heights higher than the published values. The calibrated SWAN model EVA values forced with the ECMWF-ERA5 and the calibrated SWAN model EVA values forced with the DOWA database are in the same order of magnitude; between 8.5% and 14.1% for the 2.5 km fine grid and between 12.9% and -5.4% for the 7.5 km coarse grid when compared to the EVA values calculated from the measured data. The uncalibrated ECMWF-ERA5 forced SWAN model EVA values show the worst comparison to the published values for both fine and coarse grids while the uncalibrated DOWA forced SWAN model shows the best comparison for both grid sizes.

### 4.3. Model 3: Nested Grids

#### 4.3.1. Geographical Extent and Setup

Here, we describe the relative model accuracy for the calibrated and uncalibrated model forced with the ECMWF-ERA5 and DOWA wind databases for a nested SWAN model. Note that, for consistency, the 5.0 km × 5.0 km calibrated and uncalibrated SWAN models are used (refer to Section 3.1) and nested grids are added to the models. As such, the model was not re-calibrated given the nested grids. Rather, the aim is to see if the nesting of grids improves the accuracy of the results.

The grids used in the nesting of the SWAN model follow a 1:5 ( $\rho_5$ ) decrease in average grid size; i.e., the parent grid (“coarse”) is on average a 5 km × 5 km grid, the 1st nested grid is a 1 km × 1 km resolution grid (“medium”) and the smallest grid resolution approximately 200 m × 200 m (“dense”) grid. The medium grid is orientated with the coarse grid while the dense grid is orientated parallel to the Belgium coast. The geographical extents of the grid setups are shown in Figure 16.

The various model results are again described in terms of the computed statistical parameters, i.e., mean significant wave height, RMSE, bias and correlation coefficient (Appendix B). Tables 11 and 12 show the calibrated nested SWAN model forced with the ECMWF-ERA5 and DOWA wind databases, respectively, while Tables 13 and 14 show the uncalibrated nested SWAN model statistics forced with the ECMWF-ERA5 and DOWA wind databases, respectively. Note that for each table the grids are arranged from coarse to medium to dense and compared to each other per statistical parameter.

**Table 11.** Calibrated SWAN model forced by the ECMWF-ERA5 wind database showing the mean wave heights, RMSE, Bias and correlation coefficient relative to measured data at Belgian coastal measuring stations.

Calibrated ECMWF-ERA5	Mean Significant Wave Height (m)				RMSE (m)			Bias (m)			Corr Coeff (-)		
	Mea- sured	Coarse	Med	Dense	Coarse	Med	Dense	Coarse	Med	Dense	Coarse	Med	Dense
AKZ	1.03	0.98	0.96	0.90	0.20	0.21	0.26	0.05	0.07	0.14	0.95	0.95	0.94
KWI	1.00	0.95	0.93	0.86	0.19	0.20	0.25	0.05	0.07	0.14	0.95	0.95	0.95
OSN	0.93	0.89	0.86	0.81	0.18	0.19	0.23	0.04	0.07	0.12	0.95	0.95	0.95
SWI	0.54	0.68	0.67	0.61	0.16	0.15	0.14	-0.13	-0.12	-0.07	0.70	0.71	0.72
TRG	0.59	0.64	0.59	0.58	0.18	0.17	0.16	-0.05	-0.01	0.00	0.91	0.91	0.92
WDL	0.75	0.86	0.83	0.78	0.17	0.16	0.16	-0.10	-0.08	-0.02	0.82	0.83	0.82
WHI	1.12	1.01	0.99	0.94	0.24	0.26	0.31	0.10	0.13	0.17	0.91	0.91	0.90

**Table 12.** Calibrated SWAN model forced by the DOWA wind database showing the mean wave heights, RMSE, Bias and correlation coefficient relative to measured data at Belgian coastal measuring stations.

Calibrated DOWA	Mean Significant Wave Height (m)				RMSE (m)			Bias (m)			Corr Coeff (-)		
	Mea- sured	Coarse	Med	Dense	Coarse	Med	Dense	Coarse	Med	Dense	Coarse	Med	Dense
AKZ	1.03	1.02	0.99	0.94	0.19	0.20	0.23	0.02	0.04	0.09	0.95	0.95	0.94
KWI	1.00	1.00	0.97	0.92	0.17	0.18	0.20	0.01	0.03	0.08	0.96	0.96	0.95
OSN	0.93	0.93	0.90	0.85	0.16	0.17	0.18	0.00	0.03	0.08	0.96	0.96	0.96
SWI	0.54	0.72	0.71	0.65	0.17	0.16	0.13	-0.18	-0.17	-0.11	0.71	0.72	0.74
TRG	0.59	0.70	0.64	0.63	0.20	0.18	0.15	-0.11	-0.06	-0.05	0.93	0.91	0.94
WDL	0.75	0.90	0.87	0.81	0.18	0.16	0.15	-0.14	-0.12	-0.06	0.83	0.83	0.83
WHI	1.12	1.08	1.05	1.02	0.19	0.21	0.24	0.04	0.07	0.10	0.92	0.91	0.90

**Table 13.** Uncalibrated SWAN model forced by the ECMWF-ERA5 wind database showing the mean wave heights, RMSE, Bias and correlation coefficient relative to measured data at Belgian coastal measuring stations.

Uncalibrated ECMWF-ERA5	Mean Significant Wave Height (m)				RMSE (m)			Bias (m)			Corr Coeff (-)		
	Mea- sured	Coarse	Med	Dense	Coarse	Med	Dense	Coarse	Med	Dense	Coarse	Med	Dense
AKZ	1.03	0.93	0.91	0.85	0.23	0.24	0.29	0.10	0.13	0.18	0.95	0.95	0.94
KWI	1.00	0.90	0.88	0.82	0.22	0.23	0.28	0.10	0.12	0.18	0.95	0.95	0.95
OSN	0.93	0.84	0.82	0.77	0.21	0.22	0.26	0.09	0.11	0.16	0.95	0.95	0.95
SWI	0.54	0.64	0.63	0.58	0.15	0.15	0.14	-0.10	-0.09	-0.04	0.70	0.70	0.72
TRG	0.59	0.60	0.56	0.55	0.17	0.18	0.17	-0.02	0.03	0.03	0.91	0.91	0.92
WDL	0.75	0.81	0.79	0.74	0.16	0.16	0.18	-0.06	-0.04	0.02	0.82	0.82	0.82
WHI	1.12	0.96	0.94	0.90	0.28	0.30	0.35	0.16	0.18	0.22	0.91	0.91	0.90

**Table 14.** Uncalibrated SWAN model forced by the DOWA wind database showing the mean wave heights, RMSE, Bias and correlation coefficient relative to measured data at Belgian coastal measuring stations.

Uncalibrated DOWA	Mean Significant Wave Height (m)				RMSE (m)			Bias (m)			Corr Coeff (-)		
	Mea- sured	Coarse	Med	Dense	Coarse	Med	Dense	Coarse	Med	Dense	Coarse	Med	Dense
AKZ	1.03	1.13	1.10	1.05	0.23	0.21	0.21	-0.10	-0.07	-0.01	0.95	0.95	0.94
KWI	1.00	1.11	1.08	1.02	0.21	0.20	0.18	-0.11	-0.08	-0.02	0.96	0.96	0.96
OSN	0.93	1.03	1.00	0.94	0.21	0.19	0.16	-0.10	-0.07	-0.01	0.96	0.96	0.96
SWI	0.54	0.81	0.79	0.72	0.24	0.23	0.17	-0.26	-0.25	-0.18	0.71	0.72	0.74
TRG	0.59	0.77	0.71	0.70	0.26	0.22	0.19	-0.19	-0.13	-0.12	0.93	0.91	0.94
WDL	0.75	1.00	0.97	0.91	0.26	0.23	0.18	-0.25	-0.22	-0.15	0.83	0.83	0.83
WHI	1.12	1.20	1.17	1.13	0.19	0.19	0.22	-0.08	-0.05	-0.02	0.92	0.91	0.90

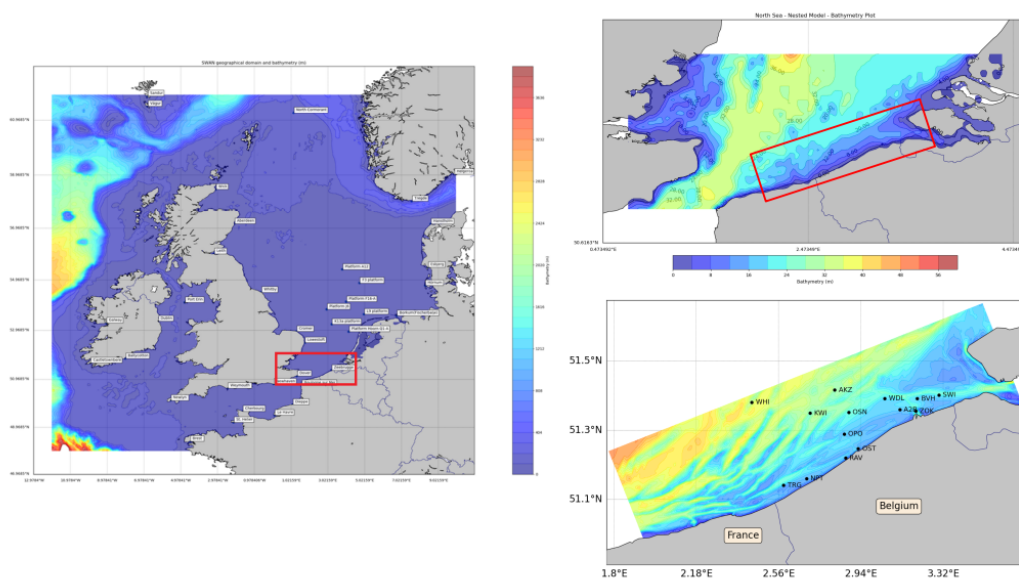


**Figure 16.** Geographical extents of the nested grids: Coarse grid shown in left panel; Medium grid shown in top-right panel; and the Dense grid in the bottom-right panel).

#### 4.3.2. Computational Statistical Comparison

Considering the statistical analysis for the calibrated SWAN models (presented in Tables 11 and 12), it can be seen that the model forced with the DOWA database shows the best results in terms of the RMSE and the average significant wave heights. In both the SWAN models forced with the ECMWF-ERA5 and DOWA winds, the average significant wave heights decrease and diverge away from the average measured values with a decrease in the grid size except for the shallow water stations SWI, TRG and WDL (i.e. shallower water and closer to the coast than the other stations). These three stations also appear to show a fairly constant RMSE for ECMWF-ERA5 forced SWAN model and a decrease in the RMSE for the SWAN model forced with the DOWA wind database while the average significant wave height shows convergence towards the average measured significant wave heights. For all other deeper water stations (AKZ, KWI, OSN and WHI), the RMSE seems to increase by between 5 cm and 7 cm from the coarse grid to the dense grid for the ECMWF-ERA5 forced SWAN model results and between 2 cm and 5 cm for the DOWA forced SWAN model results.

A similar pattern is observed for the uncalibrated models (presented in Tables 13 and 14) when compared with the calibrated models. However, the uncalibrated DOWA forced SWAN model shows an overestimation of the average significant wave height for the coarse grid in all of the stations but shows a convergence toward the measured average significant wave heights with a decrease in the grid density. In addition, the RMSE shows an improvement (decrease) with a decrease in the grid size from coarse to dense.

### 5. Discussion

Comparing model results with measurements visually (line graphs), the SWAN model is very capable of modelling the wave parameters given various calibration parameters and wind input. Very few differences are observed in this manner. However, considering the statistical analysis for *significant wave height*, it is clear that an added advantage in terms of the RMSE, at the most 10 cm, is gained from a calibrated numerical model relative to an uncalibrated model. A calibrated model forced with the DOWA wind database has a small advantage over the calibrated SWAN model forced with the ECMWF-ERA5 database with an improvement in the RMSE in the order of 2 cm. In particular, calibration of the numerical model does not significantly improve the model results in terms of significant wave height RMSE (or other statistical parameters) when compared to the SWAN model run with the default (recommended) wind formulation and white capping settings when compared with station measurements along the Belgian coast. Both databases produce the same order of results with the ECMWF-ERA5 forced uncalibrated SWAN model producing marginally better results than a SWAN model forced with the DOWA database. The reverse is true for the calibrated models (DOWA forced SWAN model is marginally better than ECMWF-ERA5 forced model). In essence, no discernible difference is seen in the accuracy between the SWAN model forced with the ECMWF-ERA5 database and the SWAN model forced with the DOWA database when comparing the wave statistics.

Considering the modelled vs. measured wave directions, the SWAN model results clearly disagree with the measured directional data with regards to the dominant spectral peak wave direction. Keep in mind that the SWAN models in the study are, by definition, purely driven by the wind database's velocities and directions which model the waves generated by the wind reflected in the wind databases. The wind-driven forcing imposed on the model seems to produce a relatively accurate record of significant wave heights but reports an overall misalignment of the dominant wave directions when compared to measured data.

The spectral peak of the SWAN modelled wave energy is underestimated in most of the analysed cases relative to measured spectral wave data. However, the tail of the spectra is shown to be well represented by the SWAN modelled data. This is an important result when providing modelled boundary conditions for models where the high-frequency tail is an important aspect (e.g., sediment models). Note that the measured wave data is not

considered accurate at low frequencies beyond 0.05 Hz. As such, not much discussion is relevant apart from the peak energy and, to a limited extent, the tail of the spectrum.

The calculated EVA values for the SWAN models underestimate the calculated measured data EVA values. This confirms the result by Cavaleri (2009) [13] pointing out that SWAN wind models fail to simulate the peak wave heights of significant storm events. The calibrated SWAN models show consistent results when the EVA values of the models forced with the ECMWF-ERA5 and DOWA databases are compared with each other, i.e., they seem to calculate EVA values within the same order of magnitude. However, the ECMWF-ERA5 forced SWAN model shows a marginally more accurate estimation than the DOWA forced SWAN model when compared to the measured data EVA values. The calculated EVA values for the uncalibrated SWAN models forced with the ECMWF-ERA5 and DOWA databases vary significantly relative to each other and to the measured data EVA values. Even though the DOWA forced SWAN model calculated EVA values show the best fit relative to the measured data EVA values, an uncalibrated SWAN model introduces additional uncertainties into the results. A counterintuitive result showed that the SWAN model (coarse 7.5 km grid, uncalibrated model forced with the DOWA wind database) is the most accurate in terms of the EVA calculations.

For nested grid simulations, a difference in the results for deeper water stations is observed relative to the shallower water stations, i.e., in terms of the RMSE, the coarse grid shows the most accurate results and becomes less accurate as the grid size decrease whereas the shallower coastal stations show an improvement as the grid size decreases. It is pertinent to note that the increase in the RMSE is in the order of 2 cm to 7 cm which translates to a general increase in the relative error of between 4% and 7% in the significant wave height for waves averaging  $H_s = 1.0$  m. In other words, for offshore stations, the relative RMSE error increases by a relatively small amount but a decrease in the relative RMSE is seen in the shallower stations. Of course, the coastal bathymetry along the Belgian coast is an important factor to consider due to the locations of the various shallow sandbanks and the relative location of the measuring stations in relation to these sandbanks. As such, it is intuitive that a finer resolution grid will have an influence on shallower stations where wave transformations (shoaling, breaking, diffraction, etc.) around these artefacts are important factors.

## 6. Conclusions

Comparing the calibrated and uncalibrated model results, it can be concluded that the uncalibrated SWAN model settings produced relatively accurate results regardless of the wind database used to force the model. Improvements in the RMSE for the calibrated model relative to the uncalibrated model can be achieved through the meticulous calibration of the numerical model; however, in this study, it was shown that a calibrated numerical model only improves the relative error by a small margin compared to the uncalibrated numerical model.

From this study, it can be concluded that a calibrated SWAN model does, in general, produce more accurate results when compared to measured data for stations along the Belgian coastline even though not by any significant margin. However, a calibrated model is only possible if adequate and sufficient measurements are available to compare the model results and to be able to calibrate the models. In the absence of available measured results, this study has shown that uncalibrated model results are reliable provided that the numerical and physical tuning parameters in the published literature are adopted in the models.

Comparing the two wind databases, within the context of wind-wave generation along the Belgian coast, it can be concluded that the SWAN models forced with the databases produce very similar results in terms of wave parameter statistics. On the modelling scale conducted in this study, there is no advantage observed in using a spatially finer scale wind database (DOWA) over a relatively coarser wind database (ECMWF-ERA5). In essence, when a limited amount of wind input databases are available, a calibrated

wind-wave model with the available database is sufficient within the context of engineering design activities.

The question of computational grid sizes vs. the wind grid size used as input to the SWAN spectral model shows no real significant benefit using a small grid resolution when comparing the RMSE for the finer (2.5 km) computational grid with the coarser 5.0 km resolution grid. A small improvement in the order of 1 cm–2 cm is seen for the calibrated models for SWAN models forced with the ECMWF-ERA5 and the DOWA wind databases, respectively. There is a more significant improvement from the uncalibrated to the calibrated model than from the coarser to the finer computational grids. The same argument seems to be true for the LTEVA calculations for the deeper water station Westhinder (WHI) where it is shown that the 7.5 km resolution coarse grid showed a better comparison to measured and published LTEVA values than the finer 2.5 km resolution grid. It can be concluded that the additional computational time required for the finer grid does not produce any notable benefit in terms of an increase in the accuracy of the results when it comes to large-scale wind-driven regional spectral wave modelling. However, a benefit to the practise of grid nesting is demonstrated when considering complex bathymetric effects that have an influence on wave transformation in the shallower areas of the coast, especially along the Belgian coastline demarcated with its numerous sandbanks.

**Author Contributions:** Conceptualization, methodology, software, validation, formal analysis, investigation, writing—original draft preparation, F.v.E.; writing—review and editing, G.K., J.V. and P.T.; supervision, P.T. and A.D.W.; project administration, funding acquisition, A.D.W. All authors have read and agreed to the published version of the manuscript.

**Funding:** This research was funded by the Coastal Division, Agency for Maritime and Coastal Services (MDK), Flemish Ministry of Mobility and Public Works, under project No. 216.055, “Creation and validation of: geodetic and tidal datums, acquisition tools at sea and in the intertidal zone”.

**Institutional Review Board Statement:** Not applicable.

**Informed Consent Statement:** Not applicable.

**Data Availability Statement:** The data presented in this study are available on request from the corresponding author.

**Acknowledgments:** The data from the Belgian wave gauges were provided by the Agency for Maritime and Coastal Services (MDK) (<https://meetnetvlaamsebanken.be/>, accessed on 16 July 2022). The authors are thankful to MDK for their continued support in this study. The authors thank the reviewers for their comments that helped to improve the quality of this paper.

**Conflicts of Interest:** The authors declare no conflict of interest.

## Abbreviations

The following abbreviations are used in this manuscript:

MDK	Agentschap Maritieme Dienstverlening en Kust (MDK) (Dutch) <i>Flemish Agency for Maritime Services and Coast (English)</i>
ECMWF	European Centre for Medium-Range Weather Forecasts
ECMWF-ERA5	ECMWF Reanalysis version 5
DOWA	Dutch Offshore Wind Atlas
NOAA	National Oceanic and Atmospheric Administration
KNMI	Koninklijk Nederlands Meteorologisch Instituut (Dutch) <i>Royal Netherlands Meteorological Institute (English)</i>
EVLTA	Extreme Value Long Term Analysis
GEVA	General Extreme Value Analysis
LGEVA	Linearised General Extreme Value Analysis
EVA	Extreme Value Analysis
MSL	Mean Sea Level

### Appendix A. Parametrise Wind-Wave Growth from $u_{10}^*$

Janssen [9] concludes that wave age, wind gusts and the wave phase speed to wind friction velocity relationship ( $c_{ph}/\bar{u}_*$ ) are important factors in calculating the wind-wave growth. In order to parametrise the wind-wave growth, Janssen introduces the background roughness length  $z_0$ , that accounts for momentum loss due to factors not considered explicitly (Charnock’s relation  $z_0 = \alpha_c \bar{u}_*^2/g$ ). In addition, the log-profile wind velocity, which introduces a roughness length  $z_1$  as follows:

$$\bar{u}_0(z) = \frac{\bar{u}_*}{\kappa} \log\left(\frac{z + z_1}{z_0 + z_1}\right) \tag{A1}$$

that represents the effect of gravity waves on the wind profile, is assumed which simplifies the parametrisation of the wind-wave growth. Thus, following the scaling arguments presented by Miles [33], the growth rate  $x$  can be expressed in terms of the dimensionless phase speed  $\bar{u}_*/c_{ph}$ , adjusted for the relative wind/wave angle  $\cos(\theta - \theta_{wind})$

$$x = \frac{\bar{u}_*}{c_{ph}} \cos(\theta - \theta_{wind}) \tag{A2}$$

and a profile parameter  $\Omega_m$  that is essentially Charnock’s relation and is expressed as follows:

$$\begin{aligned} (z_0 + z_1) &= \frac{\bar{u}_*^2}{g} \alpha_{CH} = \frac{\bar{u}_*^2}{g} \frac{\Omega_m}{\kappa^2} \\ \Omega_m &= g\kappa^2 \frac{(z_0 + z_1)}{\bar{u}_*^2} \end{aligned} \tag{A3}$$

The profile parameter  $\Omega_m$  relates the roughness of the airflow ( $z_0 + z_1$ ) and the sea state to the wave growth rate.

A final factor that must be accounted for is the so-called Miles parameter that considers the dimensionless critical height  $\mu = kz_c$ , given a logarithmic wind profile, as follows:

$$\begin{aligned} \beta &= \frac{\beta_m}{\kappa^2} \mu \log^4(\mu), \text{ where } \mu < 1, \\ \mu &= \left(\frac{\bar{u}_*}{\kappa c}\right)^2 \Omega_m \exp(\kappa/x) \end{aligned} \tag{A4}$$

where  $\beta_m$  is a constant.

As such, the wind-wave growth rate  $\gamma$  is given as

$$\begin{aligned} \gamma &= \beta \epsilon x^2 \sigma \\ &= \beta \frac{\rho_a}{\rho_w} \left[ \left(\frac{\bar{u}_*}{c_{ph}}\right) \max[0, \cos(\theta - \theta_w)] \right]^2 \sigma \end{aligned} \tag{A5}$$

where  $\rho_a$  the density of the air and  $\rho_w$  the density of the water and the contribution to the wind input source term,  $S_{in} = \gamma E$  where  $E$  is variance spectrum.

### Appendix B. Statistical Evaluation Equations

#### Appendix B.1. Mean Absolute Error (MAE)

$$\mathbf{MAE} = \frac{\sum_1^N |X_o - X_m|}{N} \tag{A6}$$

where  $N$  is the number of samples,  $X_m$  the modelled values and  $X_o$  the observed (measured) values.

Appendix B.2. Root Mean Squared Error (RMSE)

$$\mathbf{RMSE} = \sqrt{\frac{1}{N} \sum_1^N (X_o - X_m)^2} \tag{A7}$$

Appendix B.3. Bias

$$\mathbf{BIAS} = \bar{X}_o - \bar{X}_m \tag{A8}$$

where  $\bar{X} = \frac{1}{N} \sum_{i=1}^N (X_i)$  is the average over the sample space.

Appendix B.4. Correlation Coefficient

$$r = \frac{\sum_1^N (X_o - \bar{X}_o)(X_m - \bar{X}_m)}{\sqrt{\sum_1^N (X_o - \bar{X}_o)^2 \sum_1^N (X_m - \bar{X}_m)^2}} \tag{A9}$$

Appendix B.5. Bias  $\theta$

$$\mathbf{BIAS}_\theta = \frac{1}{N} \sum_{i=1}^N \Theta_i \tag{A10}$$

where  $N$  is the number of samples and  $\Theta = 180 - |180 - |\theta_o - \theta_m||$ .

Appendix B.6. Root Mean Squared Error (RMSE)

$$\mathbf{RMSE}_\theta = \sqrt{\frac{1}{N} \sum_{i=1}^N \Theta_i^2} \tag{A11}$$

**Appendix C. Extreme Value Analysis: Theory**

The extreme value analysis is performed by considering the maximum of significant wave height values within a seven-day window forming a set of independent random variables, i.e.,  $Hs_n = \max\{Hs_1, Hs_2, \dots, Hs_i\}$  where  $Hs_n$  represents the 7-day maximum for the  $n$ th 7-day window, and the series of  $Hs_n$  follows some form of a distribution function. It is assumed that the weekly maximums, constructed from the significant wave height time series, follow some form of statistical distribution, unknown at this point. The *Generalized Extreme Value Distribution* (GEVA) combines the Weibull, Gumbel and Frechet distributions as follows [47]:

$$G(z) = \exp\left\{-\left[1 + \eta\left(\frac{z - \mu}{\sigma}\right)\right]^{-\frac{1}{\eta}}\right\} \tag{A12}$$

where  $1 + \eta(z - \mu)/\sigma > 0$ ,  $\sigma > 0$  and  $-\infty < \mu, \eta < \infty$ .

From Equation (A12) it can be seen that  $\eta$  is the shape parameter,  $\sigma$  is the scale parameter and  $\mu$  the location parameter [47].

For a large enough  $n$ , the distribution of  $Hs_n$  can be approximated by a member of the distributions represented by Equation (A12). As such, by inverting Equation (A12), extreme quantiles can be found as follows:

$$z_p = \begin{cases} \mu - \frac{\sigma}{\eta} [1 - \{-\ln(1 - p)\}^{-\eta}], & \text{for } \eta \neq 0 \\ \mu - \sigma \ln\{-\ln(1 - p)\}, & \text{for } \eta = 0 \end{cases} \tag{A13}$$

where  $z_p$  is related to the return period such that it is expected that  $z_p$  is exceeded every  $1/p$  years [47]. Note that Equation (A13) can graphically interpreted as a return level plot by defining  $y_p = -\ln(1 - p)$  such that

$$z_p = \begin{cases} \mu - \frac{\sigma}{\eta} [1 - (y_p)^{-\eta}], & \text{for } \eta \neq 0 \\ \mu - \sigma \ln y_p, & \text{for } \eta = 0 \end{cases} \quad (\text{A14})$$

## References

1. CIRIA. *The Rock Manual. The Use of Rock in Hydraulic Engineering*, 2nd ed.; C683; CIRIA: London, UK, 2007.
2. USACE. *Coastal Engineering Manual*; U.S. Army Corps of Engineers: Washington, DC, USA, 2006.
3. IFS Documentation CY45R1: Part II: Data assimilation. In *IFS Documentation CY45R1*; Number 2 in IFS Documentation; ECMWF: Reading, UK, 2018.
4. Komen, G.J.; Cavaleri, L.; Donelan, M.; Hasselmann, K.; Hasselmann, S.; Janssen, P.A.E.M. *Dynamics and Modelling of Ocean Waves*; Cambridge University Press: Cambridge, UK, 1994.
5. de Winter, R.C.; Sterl, A.; Ruessink, B.G. Wind extremes in the North Sea Basin under climate change: An ensemble study of 12 CMIP5 GCMs. *J. Geophys. Res. Atmos.* **2013**, *118*, 1601–1612. [[CrossRef](#)]
6. Semedo, A.; Vettor, R.; Breivik, Ø.; Sterl, A.; Reistad, M.; Soares, C.G.; Lima, D. The wind sea and swell waves climate in the Nordic seas. *Ocean Dyn.* **2015**, *65*, 223–240. [[CrossRef](#)]
7. Signell, R.P.; Carniel, S.; Cavaleri, L.; Chiggiato, J.; Doyle, J.D.; Pullen, J.; Sclavo, M. Assessment of wind quality for oceanographic modelling in semi-enclosed basins. *J. Mar. Syst.* **2005**, *53*, 217–233. [[CrossRef](#)]
8. Lewis, H.W.; Siddorn, J.; Castillo Sanchez, J.M.; Petch, J.; Edwards, J.M.; Smyth, T. Evaluating the impact of atmospheric forcing and air-sea coupling on near-coastal regional ocean prediction. *Ocean Sci.* **2019**, *15*, 761–778. [[CrossRef](#)]
9. Janssen, P.A.E.M. *The Interaction of Ocean Waves and Wind*; Cambridge University Press: Cambridge, UK, 2004.
10. Cavaleri, L.; Abdalla, S.; Benetazzo, A.; Bertotti, L.; Bidlot, J.R.; Breivik, O.; Carniel, S.; Jensen, R.; Portilla-Yandun, J.; Rogers, W.; et al. Wave modelling in coastal and inner seas. *Prog. Oceanogr.* **2018**, *167*, 164–233. [[CrossRef](#)]
11. Mass, C.F.; Ovens, D.; Westrick, K.; Colle, B.A. Does Increasing Horizontal Resolution Produce More Skillful Forecasts? The Results of Two Years of Real-Time Numerical Weather Prediction over the Pacific Northwest. *Bull. Am. Meteorol. Soc.* **2002**, *83*, 407–430. [[CrossRef](#)]
12. Cavaleri, L.; Bertotti, L. The improvement of modelled wind and wave fields with increasing resolution. *Ocean Eng.* **2006**, *33*, 553–565. [[CrossRef](#)]
13. Cavaleri, L. Wave Modeling—Missing the Peaks. *J. Phys. Oceanogr.* **2009**, *39*, 2757–2778. [[CrossRef](#)]
14. Cavaleri, L.; Alves, J.H.; Ardhuin, F.; Babanin, A.; Banner, M.; Belibassakis, K.; Benoit, M.; Donelan, M.; Groeneweg, J.; Herbers, T.; et al. Wave modelling—The state of the art. *Prog. Oceanogr.* **2007**, *75*, 603–674. [[CrossRef](#)]
15. Briceno, L.M.; Soret, A.; Wolf, J.; Jorba, O.; Baldasano, J.M. Effect of High-Resolution Meteorological Forcing on Nearshore Wave and Current Model Performance. *J. Atmos. Ocean. Technol.* **2013**, *30*, 1021–1037. [[CrossRef](#)]
16. Lavidas, G.; Venugopal, V.; Friedrich, D. Sensitivity of a numerical wave model on wind re-analysis datasets. *Dyn. Atmos. Ocean.* **2017**, *77*, 1–16. [[CrossRef](#)]
17. Booij, N.; Ris, R.; Holthuijsen, L. A third-generation wave model for coastal regions, Part I, Model description and validation. *J. Geophys. Res.* **1999**, *104*, 7649–7666. [[CrossRef](#)]
18. Zubier, K.; Gharbi, S.H. Sensitivity of a Red Sea numerical wave model to spatial and temporal resolution of forcing wind field. *Indian J. Geo Mar. Sci.* **2019**, *48*, 566–575.
19. Klonaris, G.; Van Eeden, F.; Verbeurgt, J.; Troch, P.; Constales, D.; Poppe, H.; Wulf, D. ROMS Based Hydrodynamic Modelling Focusing on the Belgian Part of the Southern North Sea. *J. Mar. Sci. Eng.* **2021**, *9*, 58. [[CrossRef](#)]
20. De Hauwere, Nathalie. Bathymetry of the North Sea, 2016. [Bathymetry of the North Sea and Adjacent Seas. Source Data: Bathymetry: EMODnet IHO Sea Areas: Marine Regions; Licensed under a Creative Commons Attribution-Noncommercial-Share Alike 4.0 License. Available online: <https://www.marinerregions.org/maps.php?album=3747&pic=115811> (accessed on 1 September 2021).
21. Komen, G.; Hasselmann, S.; Hasselmann, K. On the existence of a fully developed wind-sea spectrum. *J. Phys. Oceanogr.* **1984**, *14*, 1271–1285. [[CrossRef](#)]
22. Janssen, P. Experimental Evidence of the Effect of Surface Waves on the Airflow. *J. Phys. Oceanogr.* **1992**, *22*, 1600–1604. [[CrossRef](#)]
23. C3S. Fifth Generation of ECMWF Atmospheric Reanalyses of the Global Climate. 2017. Available online: <https://cds.climate.copernicus.eu> (accessed on 31 August 2020).
24. Berrisford, P.; Dee, D.; Poli, P.; Brugge, R.; Fielding, K.; Fuentes, M.; Kållberg, P.; Kobayashi, S.; Uppala, S.; Simmons, A. The ERA-Interim Archive Version 2.0. 2011. Available online: <http://www.ecmwf.int/en/elibrary/8174-era-interim-archive-version-20> (accessed on 15 September 2019).
25. Duncan, J.B.; Marseille, G.J.; Wijnant, I.L. *DOWA Validation against ASCAT Satellite Winds*; Technical Report TNO Report 2018 R11649; TNO: Petten, The Netherlands, 2018.
26. Duncan, J.B.; Marseille, G.J.; Wijnant, I.L. *DOWA Validation against Offshore Mast and LiDAR Measurements*; Technical Report TNO Report 2019 R10062; TNO: Petten, The Netherlands, 2019.
27. Knoop, S.; Wijnant, I. *DOWA Validation against Coastal Wind Lidar Measurements*; Technical Report TR-376; TNO: De Bilt, The Netherlands, 2019.

28. Hersbach, H.; Dee, D. ERA5 reanalysis is in production. *ECMWF Newsl.* **2016**, *147*, 7.
29. Seity, Y.; Brousseau, P.; Malardel, S.; Hello, G.; Bénard, P.; Bouttier, F.; Lac, C.; Masson, V. The AROME-France Convective-Scale Operational Model. *Mon. Weather. Rev.* **2011**, *139*, 976–991. [[CrossRef](#)]
30. Meetnet Vlaamse Banken. Available online: <https://meetnetvlaamsebanken.be/> (accessed on 29 October 2019).
31. Booij, N.; Haagsma, I.; Holthuijsen, L.; Kieftenburg, A.; Ris, R.; van der Westhuysen, A.; Zijlema, M. *SWAN Scientific and Technical Documentation*; Delft University of Technology, Delft, The Netherlands, 2019.
32. Phillips, O. On the Generation of Waves by Turbulent Winds. *J. Fluid Mech.* **1957**, *2*, 417–445. [[CrossRef](#)]
33. Miles, J. On the Generation of Surface Waves by Shear Flow. *J. Fluid Mech.* **1957**, *3*, 185–204. [[CrossRef](#)]
34. Zijlema, M.; Vledder, G.V.; Holthuijsen, L. Bottom friction and wind drag for wave models. *Coast. Eng.* **2012**, *65*, 19–26. [[CrossRef](#)]
35. Cavaleri, L.; Rizzoli, P.M. Wind wave prediction in shallow water: Theory and applications. *J. Geophys. Res. Ocean.* **1981**, *86*, 10961–10973. [[CrossRef](#)]
36. Tolman, H. Effects of numerics on the physics in a third-generation wind-wave model. *J. Phys. Oceanogr.* **1992**, *22*, 1095–1111. [[CrossRef](#)]
37. Hasselman, K. On the spectral dissipation of ocean waves due to white capping. *Bound.-Layer Meteor.* **1974**, *6*, 107–127. [[CrossRef](#)]
38. WAMDI group. The WAM model—a third generation ocean wave prediction model. *J. Phys. Oceanogr.* **1988**, *18*, 1775–1810. [[CrossRef](#)]
39. Gunther, H.; Hasselmann, S.; Janssen, P. The WAM Model Cycle 4 (Revised Version); Technical Report Rep. No. 4; Hamburg, Germany, 1992. Available online: [https://inis.iaea.org/search/search.aspx?orig\\_q=RN:26000788](https://inis.iaea.org/search/search.aspx?orig_q=RN:26000788) (accessed on 16 July 2022).
40. Van der Westhuysen, A. Advances in the Spectral Modelling of Wind Waves in the Nearshore. Ph.D. Thesis, Department of Civil Engineering, Delft University of Technology, Delft, The Netherlands, 2007.
41. Yan, L. An Improved Wind Input Source Term for Third Generation Ocean Wave Modelling; Technical Report Scientific Report WR-no 87-8; De Bilt, The Netherlands, 1987. Available online: <http://publicaties.minienm.nl/> (accessed on 16 July 2022).
42. Battjes, J.; Janssen, J. Energy loss and setup due to breaking of random waves. In Proceedings of the 16th International Conference on Coastal Engineering, Hamburg, Germany, 27 August–3 September 1978; pp. 569–587.
43. Eldeberky, Y. Nonlinear Transformation of Wave Spectra in the Nearshore Zone. Ph.D. Thesis, Delft University of Technology, Delft, The Netherlands, 1996.
44. Vuik, V.; Kuijper, B.; Geerse, C.; Strijker, B.; Gautier, C.; Trouw, K.; Vanneste, D.; Suzuki, T.; Nossent, J.; Thoon, D.; et al. Het Hydraulisch Randvoorwaardenboek Achtergrondrapport. Versie 3.0. WL Rapporten, 18\_037\_2; Technical Report 18\_037\_2; Antwerpen, 2020. Available online: <https://www.vlaanderen.be/publicaties/het-hydraulisch-randvoorwaardenboek-2020-achtergrondrapport> (accessed on 16 July 2022).
45. Pyextremes—Extreme Value Analysis (EVA) in Python. [Computer Software Source Code], Software Version 2.2.4. Available online: <https://georgebv.github.io/pyextremes/> (accessed on 15 November 2021).
46. Akaike, H. Information Theory and an Extension of the Maximum Likelihood Principle. In *Breakthroughs in Statistics: Foundations and Basic Theory*; Kotz, S., Johnson, N.L., Eds.; Springer: New York, NY, USA, 1992; pp. 610–624. [[CrossRef](#)]
47. Coles, S. *An Introduction to Statistical Modeling of Extreme Values*; Springer: London, UK, 2001.